(4)

GL-TR-90-0017

Studies of Regional Phases and Discriminants in Asia

Author(s) : Francis T. Wu

State University of New York
P. O. Box 9
Albany, New York 12201

19 January 1990

Final Report
Period Covered : 1 February, 1987 to 31 August, 1989

GEOPHYSICS LABORATORY
AIR FORCE SYSTEMS COMMAND
UNITED STATES AIR FORCE
HANSCOM AIR FORCE BASE, MASSACHUSETTS 01731-5000

0

SPONSORED BY
Defense Advanced Research Projects Agency
Nuclear Monitoring Research Office
ARPA ORDER NO.5299

MONITORED BY
Geophysics Laboratory
F19628-87-K-0007

This technical report has been reviewed and is approved for publication.

JAMES F. LEWKOWICZ
Contract Manager
Solid Earth Geophysics Branch
Earth Sciences Division

JAMES F. LEWKOWICZ
Branch Chief
Solid Earth Geophysics Branch
Earth Sciences Division

FOR THE COMMANDER

DONALD H. ECKHARDT, Director
Earth Sciences Division

This report has been reviewed by the ESD Public Affairs Office (PA) and is releasable to the National Technical Information Service (NTIS).

Qualified requestors may obtain additional copies from the Defense Technical Information Center. All others should apply to the National Technical Information Service.

If your address has changed, or if you wish to be removed from the mailing list, or if the addressee is no longer employed by your organization, please notify GL/IMA, Hanscom AFB, MA 01731-5000. This will assist us in maintaining a current mailing list.

Do not return copies of this report unless contractual obligations or notices on a specific document requires that it be returned.

Unclassified

SECURITY CLASSIFICATION OF THIS PAGE

REPORT DOCUMENTATION PAGE

1a. REPORT SECURITY CLASSIFICATION Unclassified	1b. RESTRICTIVE MARKINGS
2a. SECURITY CLASSIFICATION AUTHORITY	3. DISTRIBUTION / AVAILABILITY OF REPORT approved for public release; distribution unlimited
2b. DECLASSIFICATION / DOWNGRADING SCHEDULE	
4. PERFORMING ORGANIZATION REPORT NUMBER(S)	5. MONITORING ORGANIZATION REPORT NUMBER(S) GL-TR-90-0017
6a. NAME OF PERFORMING ORGANIZATION State University of New York 6b. OFFICE SYMBOL (If applicable)	7a. NAME OF MONITORING ORGANIZATION Geophysics Laboratory
6c. ADDRESS (City, State, and ZIP Code) P. O. Box 9 Albany, N.Y. 12201	7b. ADDRESS (City, State, and ZIP Code) Hanscom AFB Massachusetts 01731-5000
8a. NAME OF FUNDING / SPONSORING ORGANIZATION 8b. OFFICE SYMBOL (If applicable)	9. PROCUREMENT INSTRUMENT IDENTIFICATION NUMBER F19628-87-K-0007
8c. ADDRESS (City, State, and ZIP Code)	10. SOURCE OF FUNDING NUMBERS

PROGRAM ELEMENT NO.	PROJECT NO.	TASK NO.	WORK UNIT ACCESSION NO.
61102F	7A10	DA	CE

11. TITLE (Include Security Classification)
Studies of Regional Phases and Discriminants in Asia

12. PERSONAL AUTHOR(S)
Francis T. Wu

13a. TYPE OF REPORT	13b. TIME COVERED	14. DATE OF REPORT (Year, Month, Day)	15. PAGE COUNT
Final Report	FROM 2/1/87 TO 8/31/89	1990 January 19	66

16. SUPPLEMENTARY NOTATION

17. COSATI CODES			18. SUBJECT TERMS (Continue on reverse if necessary and identify by block number)
FIELD	GROUP	SUB-GROUP	Regional phases, eastern Asia, regionalization of surface waves, explosion waveforms

19. ABSTRACT (Continue on reverse if necessary and identify by block number)

The following conclusions were obtained from studies under this contract:

(1) Lg propagation in eastern Asia is fairly complex because of the presence of tectonic provinces with distinctive waves propagation characteristics.

(2) At the Chinese Kirnos stations, WMQ and KSH, high frequency Lg waves from Semipalatinsk are recorded well. At more distant stations, such as LZH and BJI, Lg amplitudes are small even for Mb>6.0 events. The low magnification of the Chinese Kirnos stations is a limiting factor.

(3) The recently installed CDSN stations provide excellent signal to noise ratios for eastern Asian events with magnitude greater than 4.5 or so across the network. Some events smaller than 4.5 may provide very clear surface waves.

(4) Regional phases are very prominently developed for paths that do not cross the Tibetan Plateau. A path with less than three hundred kilometers in the Plateau often means little discernible Lg waves.

(5) Regionalization studies of surface waves have allowed us to determine the dispersions in many tectonic provinces. This seems to be the most suitable way to determine the crustal structures of this area, with a high quality, but sparse, network.

20. DISTRIBUTION / AVAILABILITY OF ABSTRACT	21. ABSTRACT SECURITY CLASSIFICATION
☐ UNCLASSIFIED/UNLIMITED ☐ SAME AS RPT. ☐ DTIC USERS	Unclassified

22a. NAME OF RESPONSIBLE INDIVIDUAL	22b. TELEPHONE (Include Area Code)	22c. OFFICE SYMBOL
James Lewkowicz	(617) 377-3028	GL/LWH

DD FORM 1473, 84 MAR 83 APR edition may be used until exhausted. All other editions are obsolete.

SECURITY CLASSIFICATION OF THIS PAGE
Unclassified

Table of Contents

1 Introduction

The propagation of regional phases in eastern Asia, within the boundary of the People's Republic of China, is not well known because of the lack of data there up to early 1980's. Since then data from a number of the Chinese Kirnos network stations were available in 70 mm film chips. The Kirnos instruments have relatively broad frequency response, but the gains are about 1500-2000 in the frequency range from 10 Hz down to 0.1 Hz. Thus, events in the magnitude range of less than 4 are not observed at all stations. The recently installed Chinese Digital Seismic Network provides excellent data in the short-period, intermediate and long-period bands. To date data from five to six stations are available on a regular basis.

2 Regional Phases at WMQ and KSH from the Semipalatinsk test sites

2.1 Objective

Regional phases such as Sn, Lg and Rg may contain valuable information for the discrimination between earthquakes and underground nuclear tests. Film records from the broad-band Chinese Kirnos stations are available from 1979 to 1984, and for the first time we can study the propagation of regional phases across eastern Asia. In this report, we summarize results previously published in China, of regional phases observed at a number of the Kirnos stations (Fig. 2.1.1), and then provide preliminary results of our analysis of the Kirnos film records.

2.2 Summary of Chinese Results

Examples of seismograms and a brief description of them are contained in Zhao (1980). The most important observational results of regional phases are summarized as follows:

1. Within a distance of 10°: (a) In eastern China, P_n and S_n are typically weak and unclear. P^* is occasionally seen, but in western China, in Xinjiang and Tibet, P_n and S_n may be quite prominent. (b) PL waves have periods between 6 and 20 seconds.

2. Between 10° and 20°: (a) P and S waves tend to be weak or absent, (b) Lg1 and Lg2 at velocities of 3.54 km/sec and 3.38 km/sec respectively are usually observed. Lg1 appears more frequently from sources at depths greater than 10 km, while Lg2 becomes more dominant for shallower sources. Periods of Lg waves range from 0.5 to 5 seconds, mostly between 2 to 4 seconds. They may persist for more than 10 cycles. Lg however, does not propagate well across the Tibetan Plateau; the arrival within the group velocity window of 3.5 to 3.3 km/sec consist of long (10 second) period pulses.

3. Between 20° and 30°: (a) P and S waves are very clear. (b) Lg waves tend to appear with a dominant period of about 6 seconds.

2.3 Regional Phases Observed at Chinese Stations from Semipalatinsk Sources

Patton and Mills (1984) and Langston (1986) have shown the broad-band Kirnos records from Chinese stations contain clear mid-period surface waves at Urumchi stations. Currently, records from sixteen similar stations (1979 to mid-1984) are in archive at USGS office in Denver. The locations and names of these stations are shown in Fig. 2.3.1.

The Kirnos instrument response is essentially flat between 0.1 to 10 seconds. The magnification of the horizontal component at different stations varies between 1400 and 2400 with the vertical magnification about one half of the horizontal. Because of the relatively low magnification, large events (5 < Mb <6.5) are quite often recorded on scale at distances of around 1000 km. However, the wave amplitudes at more distant stations are often small, especially at the high frequency end.

We use records from a series of Semipalatinsk tests in 1980 and 1982 to study the propagation of Lg across China. Figure 2.3.2 shows the general observability of Lg2 (within a velocity window of 3.4-3.2 km/sec) of a Mb=5.9 (USGS) event. The amplitude has been corrected for instrument magnifications and is expressed in millimeters on our film reader; the noise level is about 2 mm. Event of smaller magnitude are normally observed clearly only at WMQ (epic. dist.=950 km) and KSH (epic. dist.=1160 km). At LZH (epic. dist.=2550 km) a Mb=5.4 event may be barely observable. The Lg waves at WMQ and KSH are dominated by 1 second waves while at greater epicentral distances 4 to 6 second waves are observed.

The WMQ and KSH stations provide excellent records of the Semipalatinsk events. Although the epicentral distances to these two stations differ by 200 km, the waveforms are totally different. The WMQ records consistently show an emerging Lg and dispersed Rayleigh waves, while at KSH Lg waves show an impulsive beginning and a long decaying tail without clear surface waves. The P waves are usually weak and the Lg waves are the first large amplitude waves observed. The path between WMQ and the Semipalatinsk test site is relatively flat and crosses a minor mountain range. The wave path between KSH and the test site, on the other hand, cross a major range, the Tianshan. These differences are evidently responsible for the differences in observed seismograms.

The Semipalatinsk events recorded at WMQ have common recognizable characteristics. In Fig. 2.3.3, the vertical components for five events ranging in magnitudes from 5.5 to 5.9 are shown. The high frequency Lg superposed on the 8-10 sec. period Rayleigh waves are very clearly displayed for the lower four traces, but for the 5.5 event, the high frequency is almost absent.

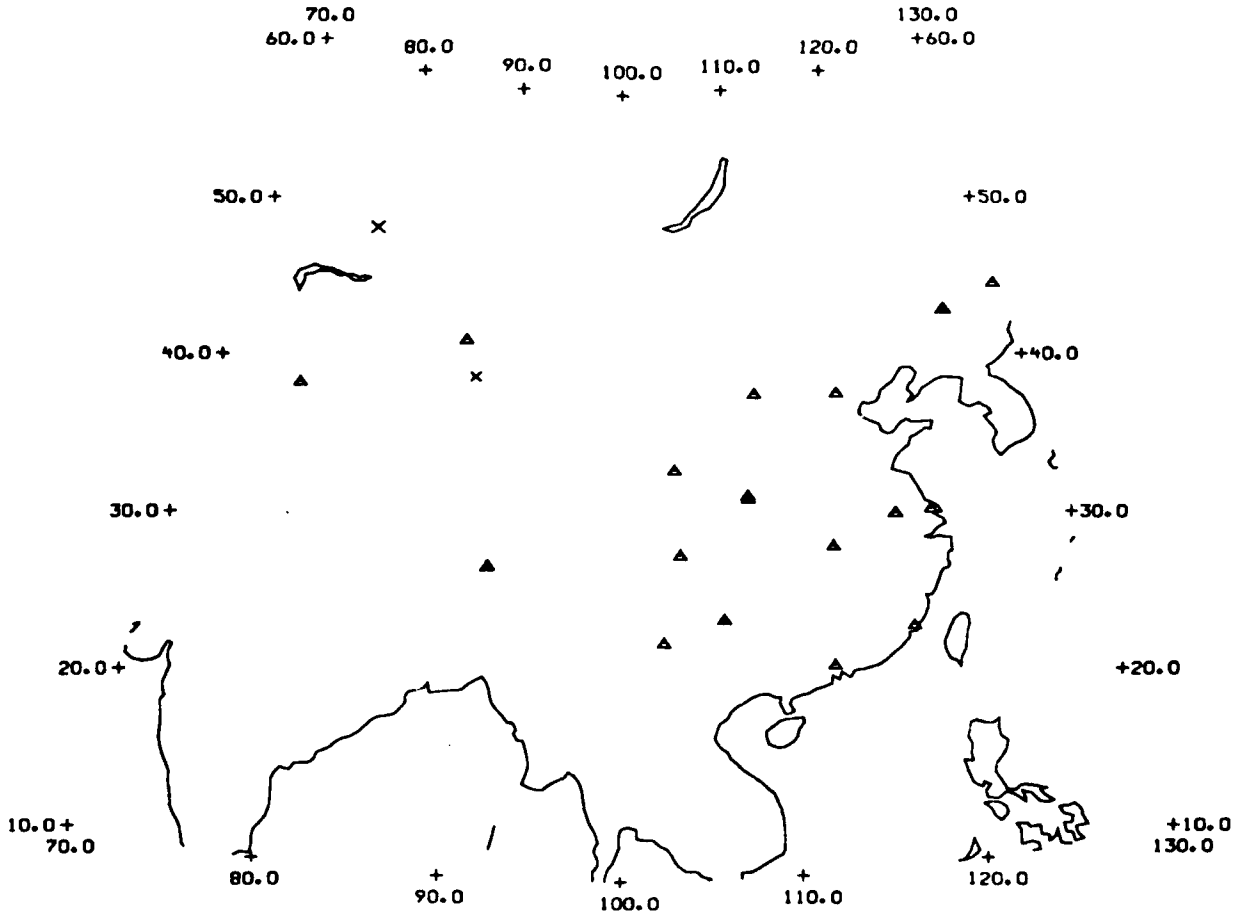

Figure 2.3.1. Location map for the Chinese Kirnos network.

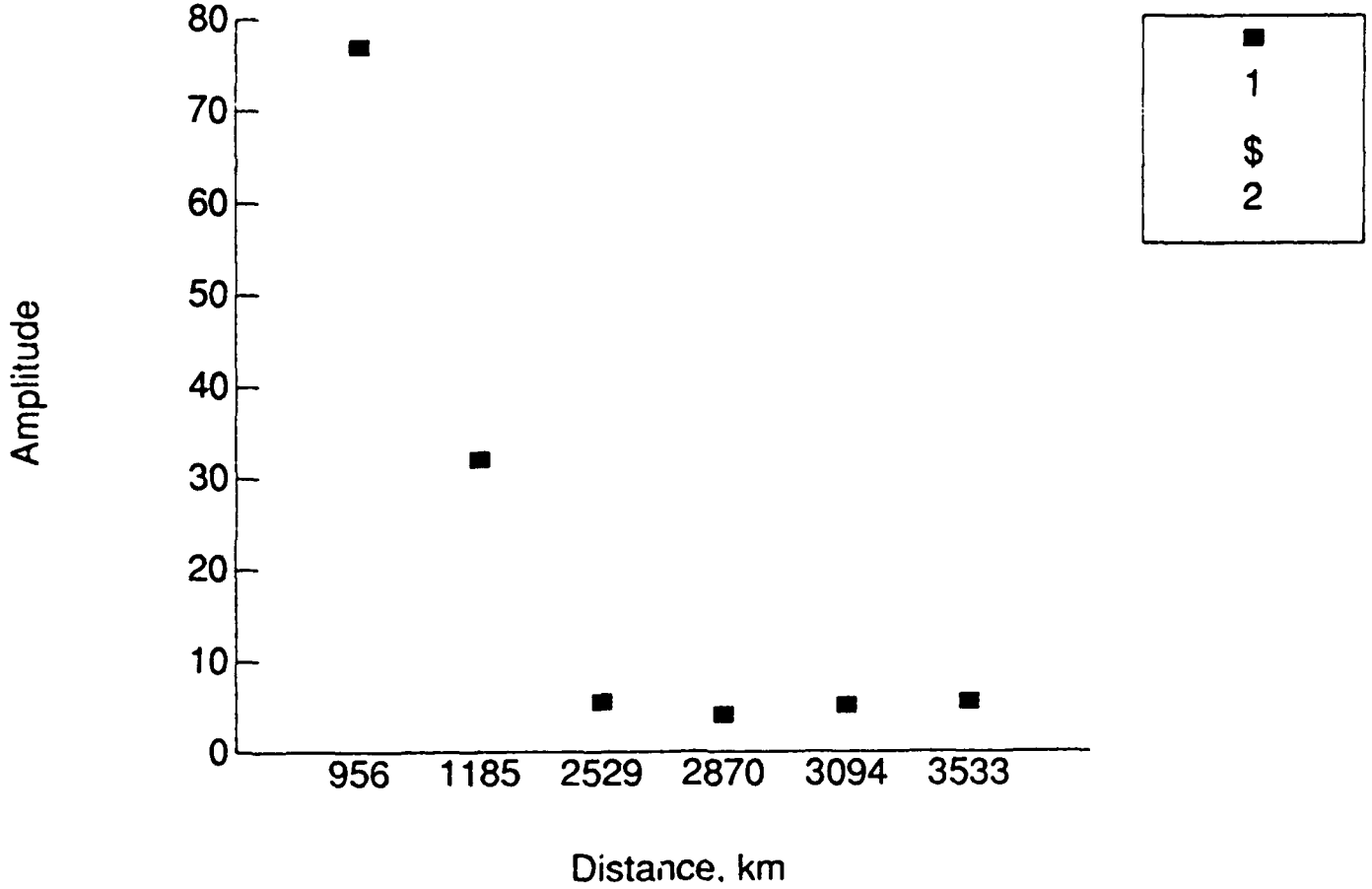

Figure 2.3.2. Observed amplitude variations across the Kirnos network from a Mb=5.9 event in E. Kazakh.

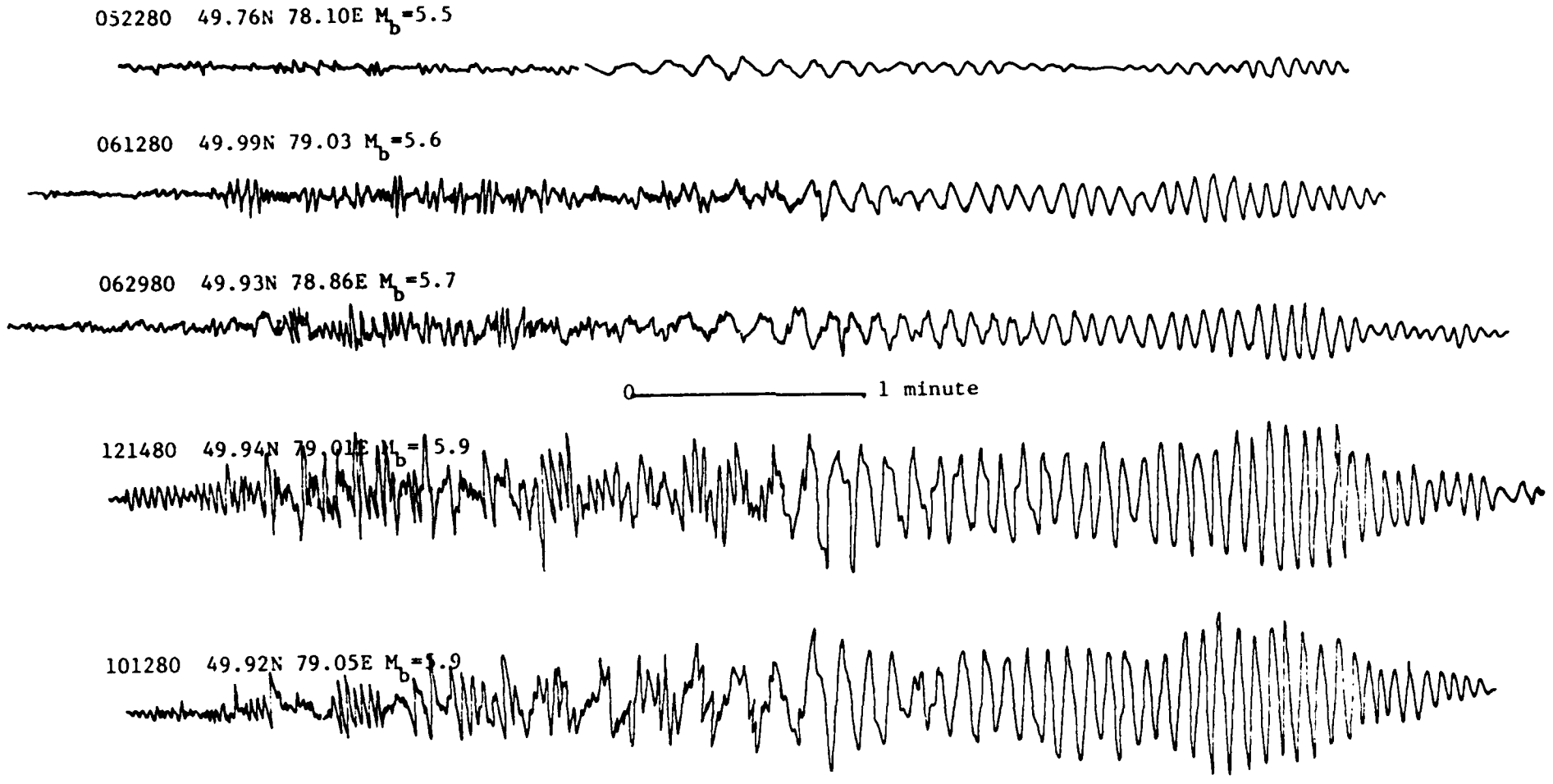

Figure 2.3.3. Vertical component WMQ seismograms for five events of different sizes from E. Kazakh.

We have measured maximum amplitudes of Lg waves on the three components as well as that of the P waves, the 8-10 seconds Rayleigh waves and the 4 second Rayleigh wave near the end of each wave train. The results are shown in Fig. 2.3.4. It is seen that the linear amplitudes increase nearly exponentially as they should, except in the case of 8-10 seconds Rayleigh waves.

2.4 Conclusions

Lg propagation in eastern Asia is fairly complex because of the presence of various tectonic provinces. At WMQ and KSH high frequency Lg waves are recorded well. At more distant stations, Lg amplitudes are small even for Mb=6.2 Semipalatinsk events. The observation is evidently limited by the low magnification of the Chinese Kirnos stations.

To get a more complete view of the regional phase propagation, earthquakes in various parts of eastern Asia recorded at the Kirnos stations should be studied. The Chinese Digital Seismic Network data is coming online. Data from this network has a much larger dynamic range and should prove to be of key importance in the whole study.

3 Regional phase observations at CDSN stations

This section shows some examples of typical earthquake and explosion seismograms recorded at several CDSN stations (Fig. 3.0.1). All events are those in 1987. The event information is shown in Table 3.1. For the CDSN records the short and intermediate components are triggered. Usually the short period records contian only the P phases and the coda. The intermediate records often include most of the Lg and later phases. To show more complete records and taking particular notice of the regional phases, we have high-pass filtered (four pole Butterworth with corner at 0.5 Hz) the intermediate components to simulate short period records. In all figures, when three component seismograms are shown, they are arranged in the order, from top down, as east-west, north-south and vertical.

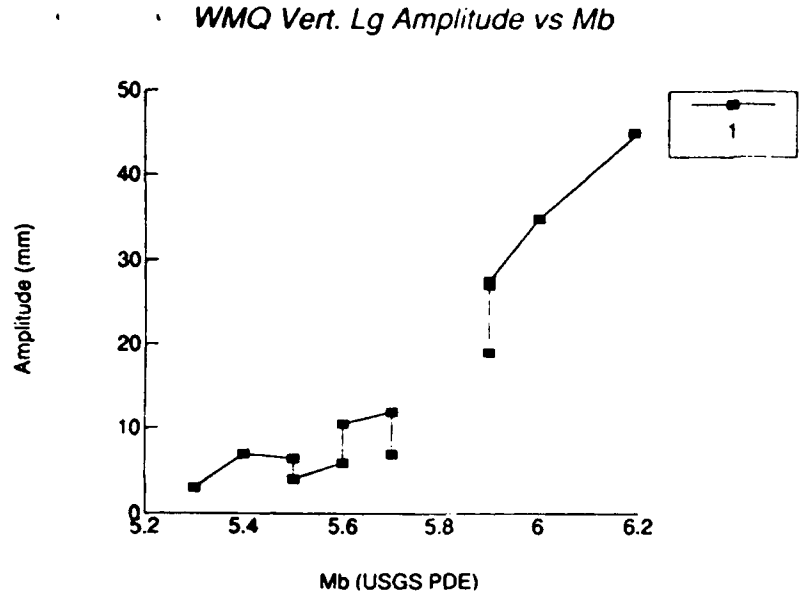

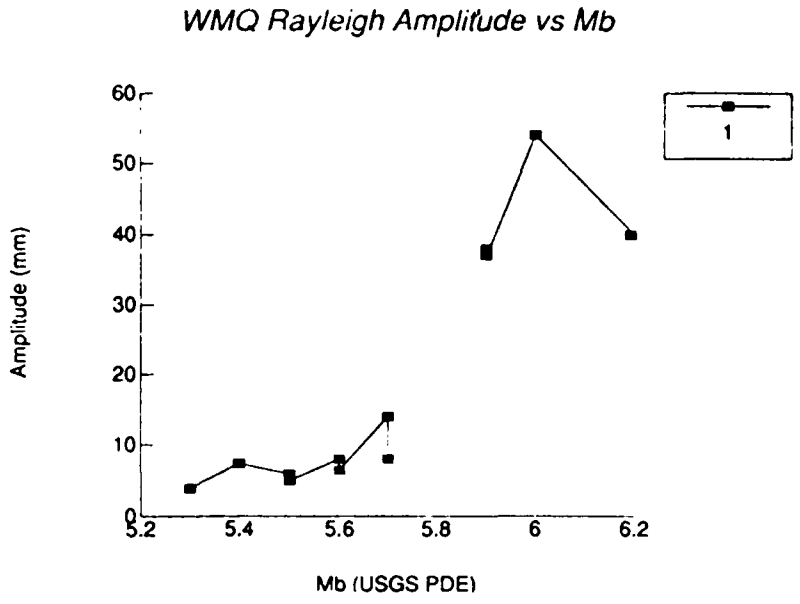

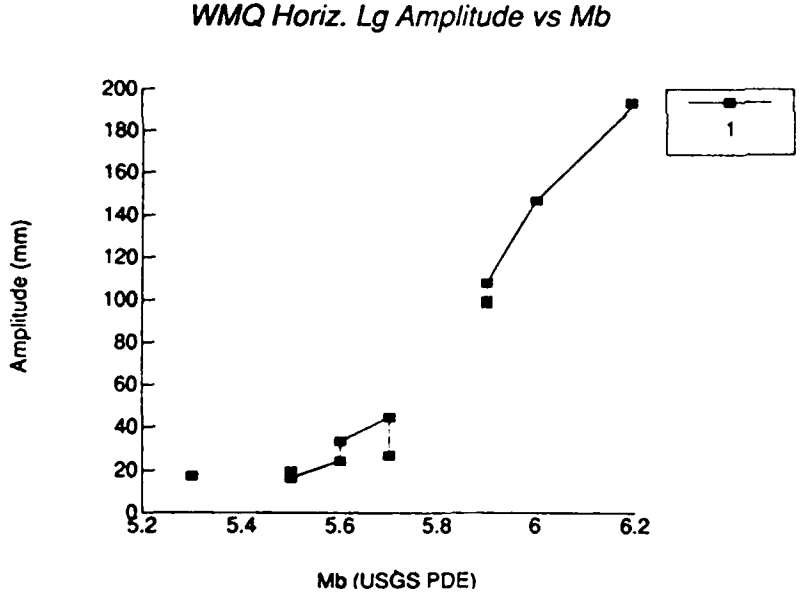

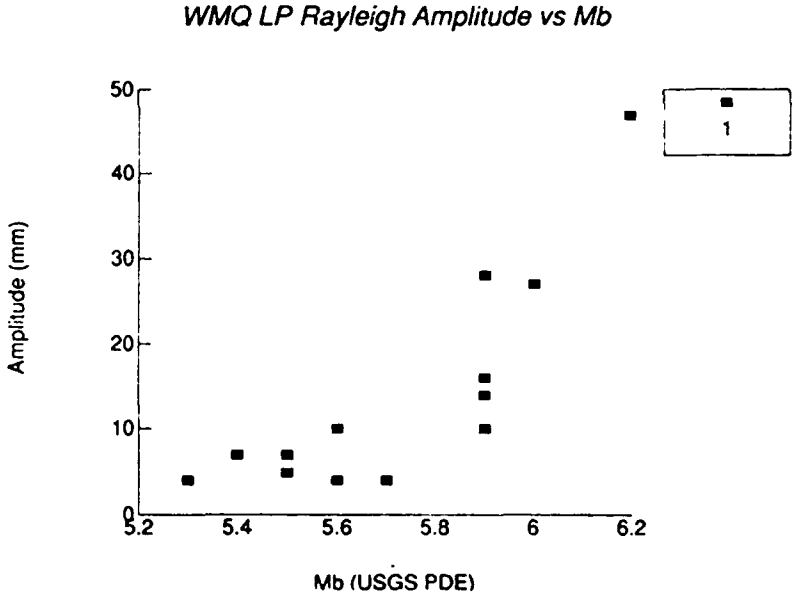

Figure 2.3.4. (a) WMQ vertical Lg amplitude vs Mb, (b) WMQ horizontal Lg vs Mb, (c) WMQ 4 second Rayleigh amplitude vs Mb, and (d) WMQ 8-10 second Rayleigh vs Mb.

...ble 3. Events information for the regional seismogrrams shown in figures 3.1 through 3.12.

Date	O. Time	Lat	Long	D (km)	Mb	Distance WMQ	LZH	BJI	KMI	Event Location	Fig No.
01/05	22:52:46.5	41.96	81.3	17	5.9	560.5				Tianshan	3.1
01/07	18:19:08.8	34.0	103.4	33	5.2	1718				S. E. Gansu	3.2
01/24	08:13:14.4	41.4	79.4	33	5.9	731.2				Tianshan	3.3
01/28	12:12:15.9	45.36	96.1	33	5.1	692.2	1217			W. Mongolia	3.4
02/25	19:56:35.5	38.1	91.2	26	5.7	699.9	1146			W. Qaidam	3.5
03/01	17:59:10.0	49.8	102.8	24	4.8	1323		1511		N. Mongolia	3.6
04/30	05:17:37.0	39.8	74.6	8	5.7	1175				S. Xinj.	3.7
06/06	02:37:07.0	49.86	78.11	0	6.1	990.8				Degelen	3.8
06/08	13:30:32.8	39.8	74.6	10	5.1	1172				S. Xinj.	3.9
06/20	00:53:04.8	49.9	78.7	0	5.5	960.3				Shagan R.	3.10
08/09	21:14:58.2	29.4	83.7	34	5.6	1628				W. Himalaya	3.11
08/10	12:12:14.1	38.19	106.4	33	5.4	1689	318.1			Yinchuan Grab.	3.12
09/06	23:38:52.2	26.7	93.4	42	5.4	1969			950.6	E. Himalaya	3.13
09/18	21:58:36.6	47.28	89.7	10	5.3	387.6				Altai Mount.	3.14
09/27	06:12:42.5	34.1	80.7	33	4.9	1228				NW Tibet	3.15
10/03	11:00:03.3	36.5	71.5	80	6.0	1604				Pamir	3.16
11/03	18:24:49.7	33.1	86.9	33	4.9	1189				C. Tibet	3.17
12/17	12:17:23.4	41.8	83.1	33	5.1	421.9				N. Tarim	3.18
12/22	00:16:39.1	41.4	89.7	21	5.9	316.1	1364			E. Tarim	3.19

Figures 3.1 through 3.19 show a series of representative seismograms recorded at three of the CDSN stations. The seismograms are intermediate-period records, unless otherwise noted in the figure caption, and have been subjected to high-pass Butterworth filter with the corner at 0.5 Hz and with four poles. Although a longer seismogram is usually available for the intermediate-period records than the short period records, often the regional phases are not complete. The trigger system on these systems need to be improved. WMQ station is the best station to look at regional phases because of the many events within a distance range f 2000 km.

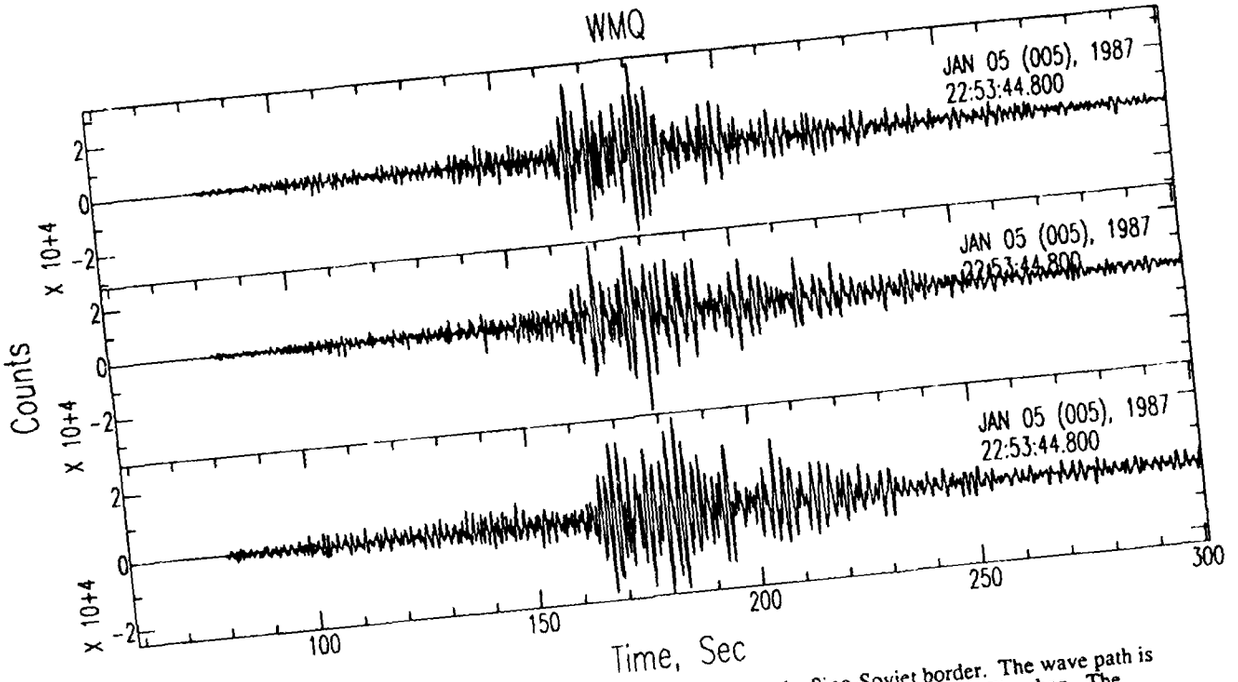

Figure 3.1 This event is located in the southern Tianshan near the Sino-Soviet border. The wave path is wholly contained within the Tianshan, since WMQ is located on the northern side of Tianshan. The waves come from the SWW direction. The Lg phase is well developed with a velocity of 3.4 km/sec for the first group and about 3.1 km/sec for the later group. For event parameters see Table 3.1. The legend on the top right of each frame shows the date of the event [Calendar day and Julian day, year] and the time corresponding to the first data point shown in the diagram. The y-axis shows the digital counts and the x-axis shows the time in seconds counted from the origin time.

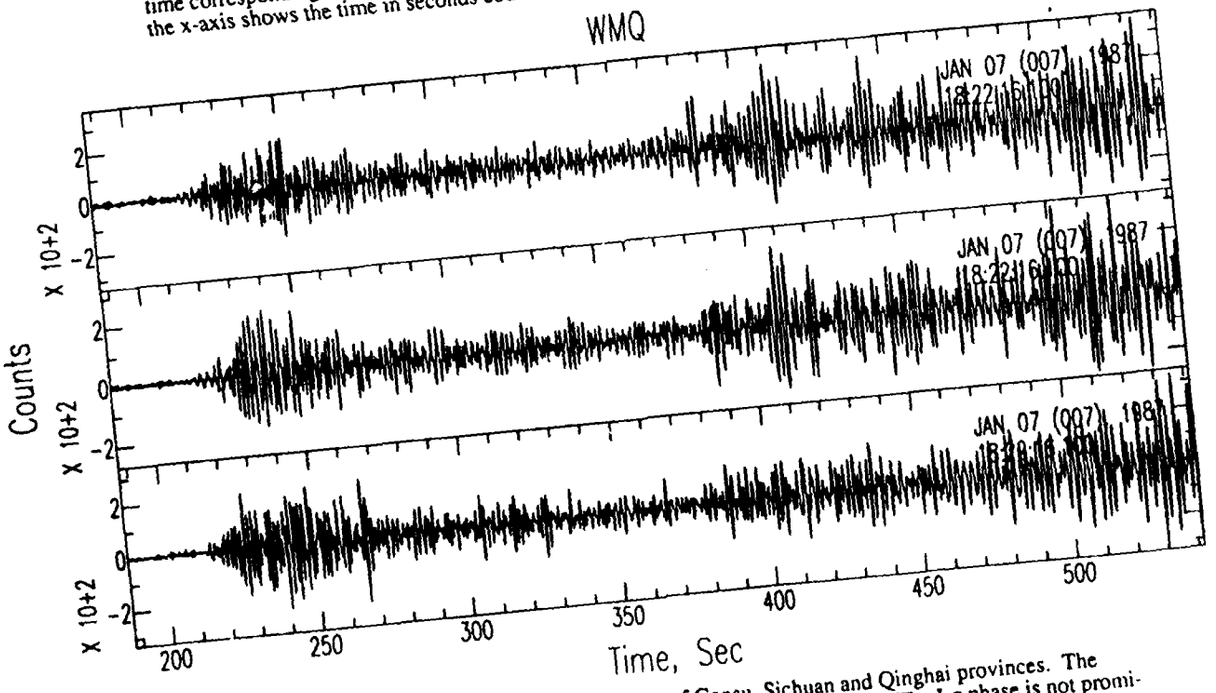

Figure 3.2 WMQ records of an event near the border of Gansu, Sichuan and Qinghai provinces. The wave path crosses the Qilian Shan, part of the Tarim Basin and the Tianshan. The Lg phase is not prominent (the 3.4 km/sec phase is expected to arrive around 500 seconds). The P and S coda are well-developed.

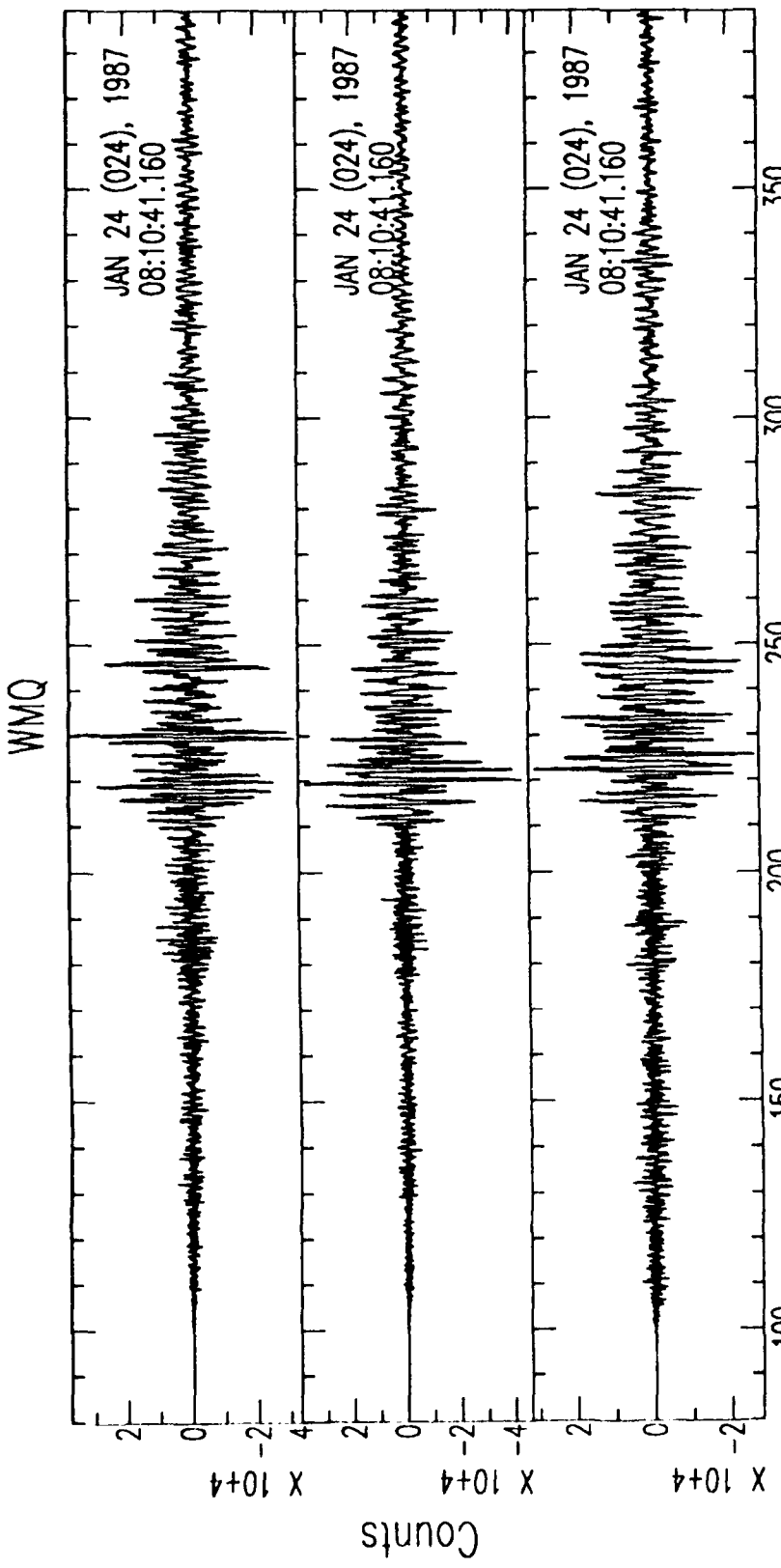

Figure 3.3 WMQ records of a southern Tianshan earthquake 170 km further west from WMQ than the event shown in figure 3.1. These two sets of records bear a great deal of resemblence. The first Lg phase again has a velocity of about 3.4 km/sec.

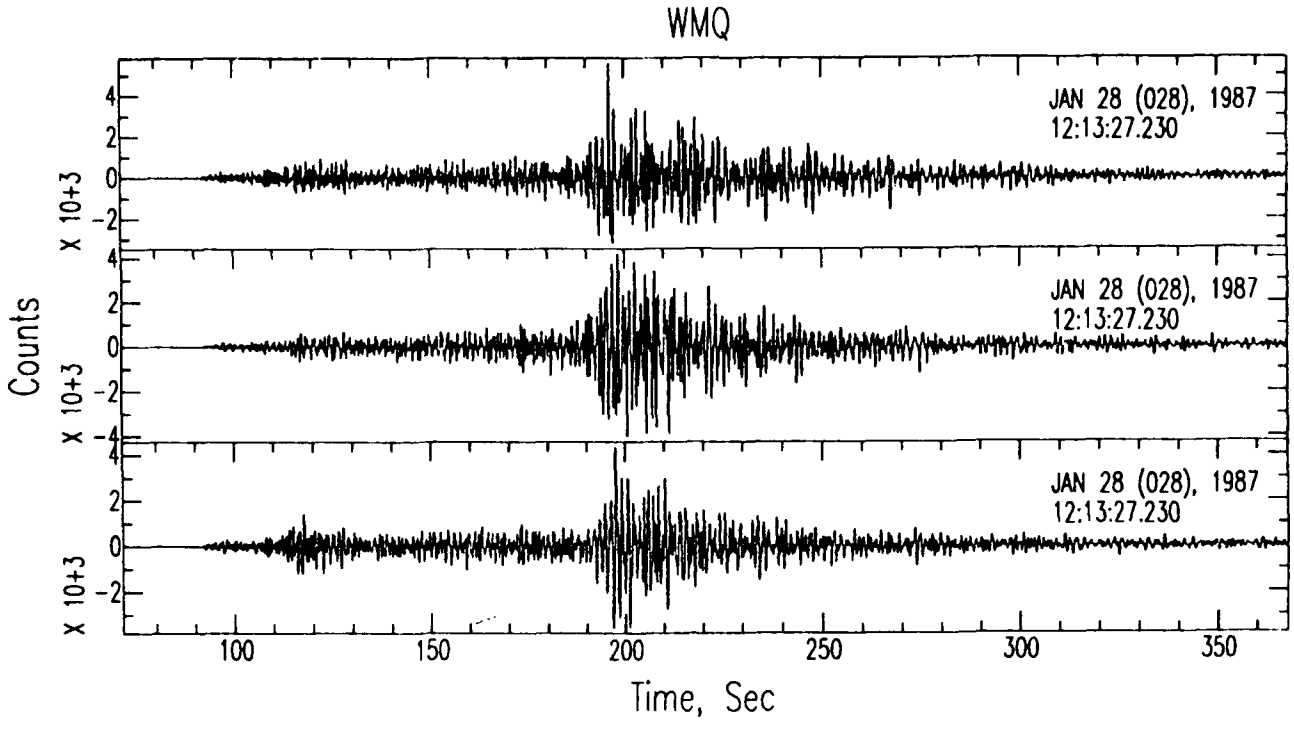

Figure 3.4 (a) WMQ and (b) LZH records of an event in western Mongolia. Lg arrives with 3.6 and 3.52 km/sec velocity at WMQ and LZH, respectively. The WMQ paths crosses the Altai Mountains while the LZH path goes along the Qilain Mountain chain.

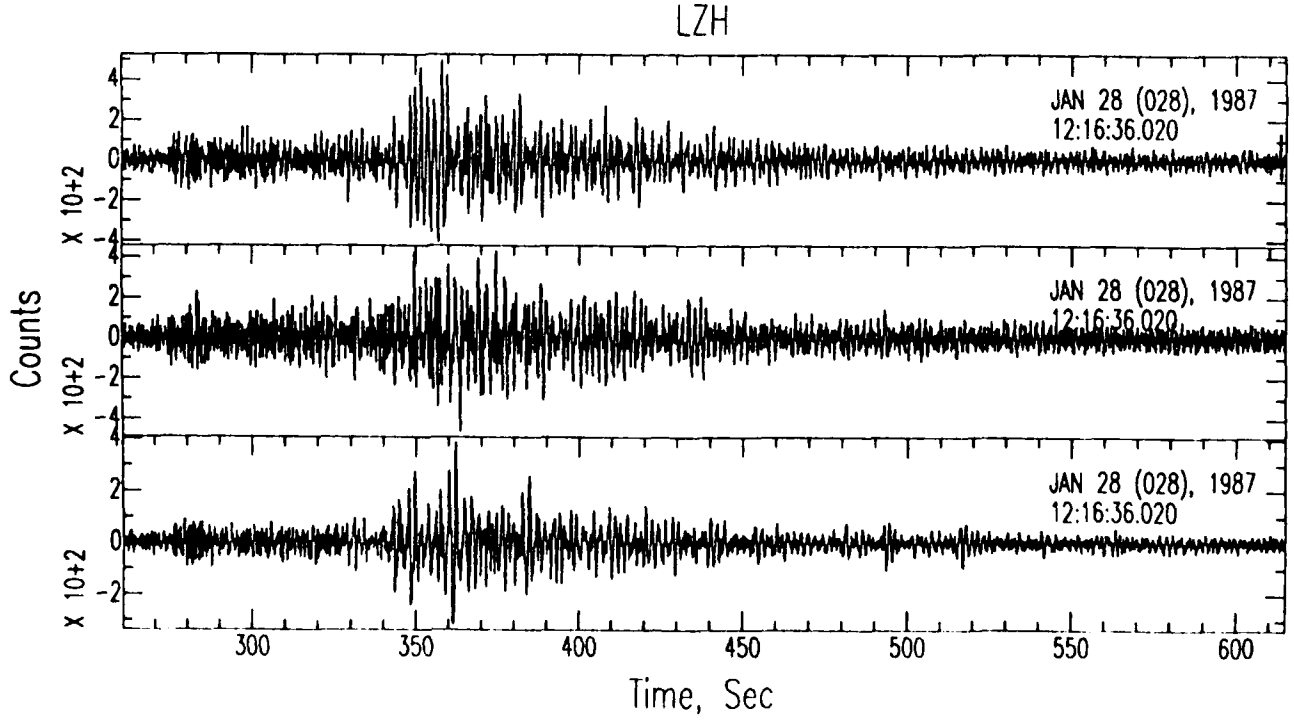

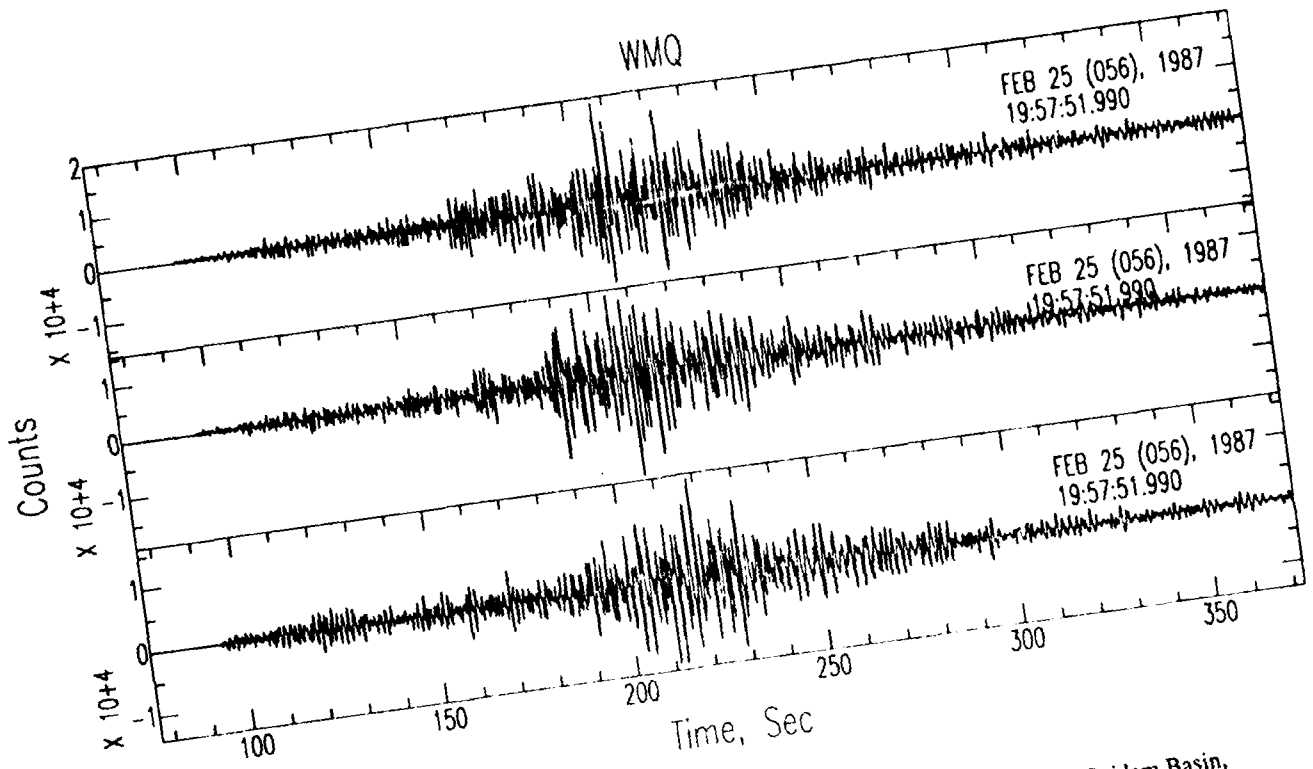

Figure 3.5 (a) WMQ and (b) LZH records from an event in the northwestern part of the Qaidam Basin, probably in the Qimantag. The wave path to WMQ lies mostly in the Tarim Basin and portions in the Tianshan and in the Altyn Tag. The first Lg phase has a velocity of about 3.5 km/sec. The path between LZH and the event lies in the Qilian Mountains of northern Gansu. The first group of Lg again has the velcity of about 3.5 km/sec and the later group, 3.05 km/sec.

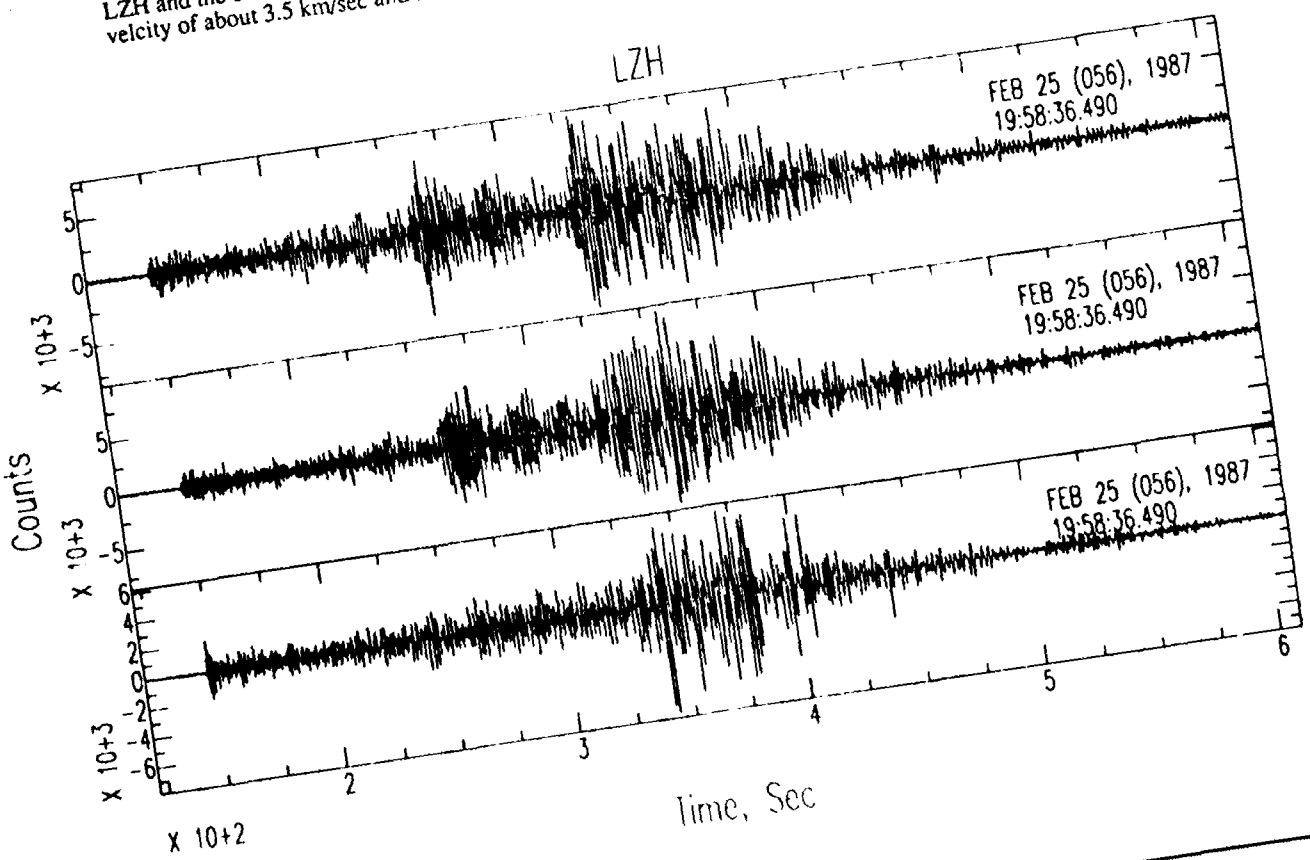

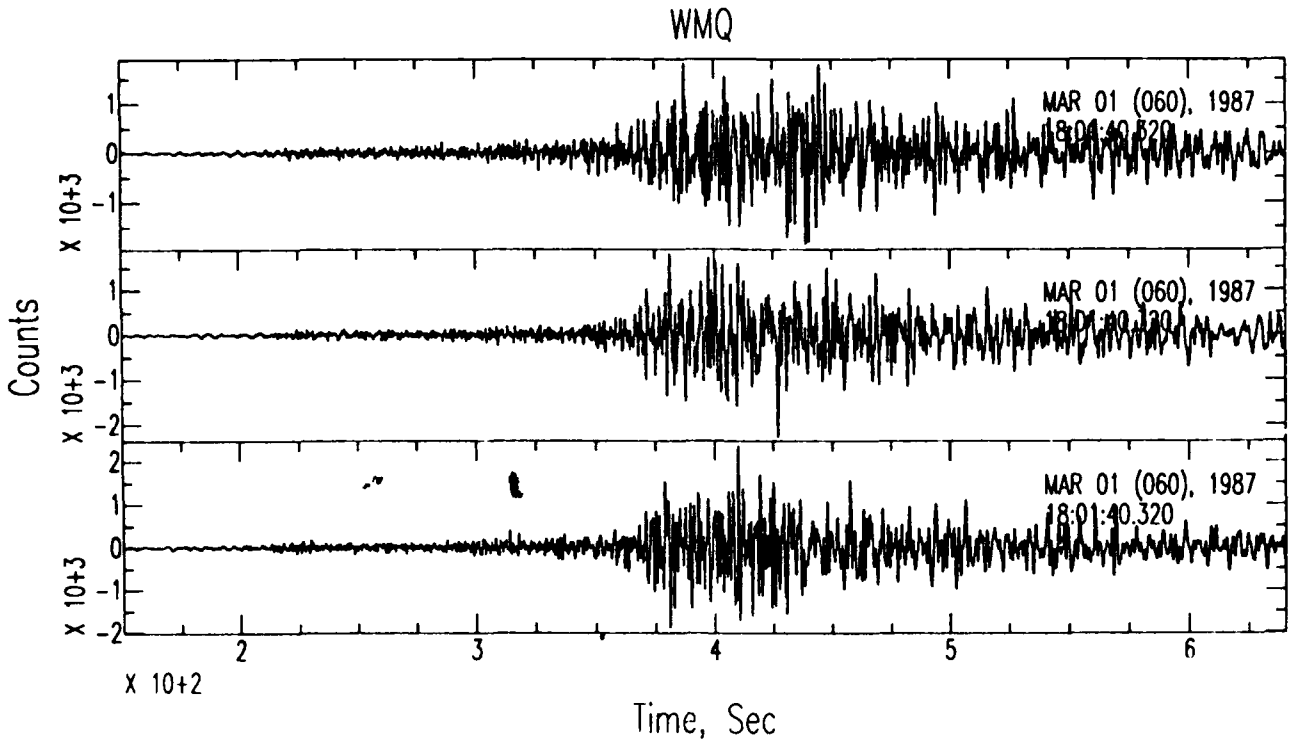

Figure 3.6 (a) WMQ and (b) BJI records from an event in northern Mongolia near the Soviet Border. While the path to WMQ crosses two mountain chains, the Changgajin in southwestern Mongolia and the Altai Mountains along the border between Mongolia and China, the path to BJI lie almost entirely within the PreCambrian Shield area of eastern Mongolia and northeastern China. The relative simplicity of the BJI records in comparison to the WMQ records can be ascribed to the pure path for the BJI path and more heterogeneous path for WMQ. The Lg waves arrive between a velocity window of 3.57 to 2.94 at WMQ and 3.5 to 3.18 at BJI.

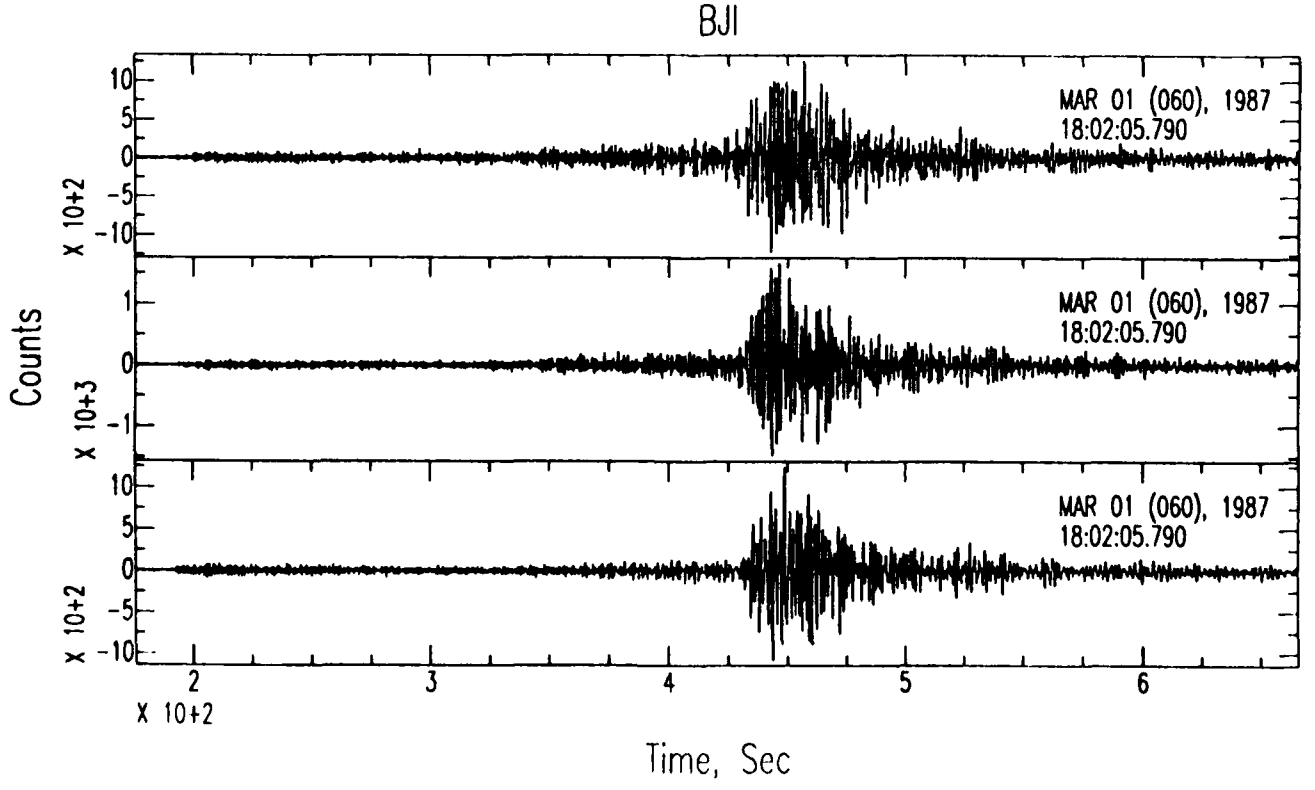

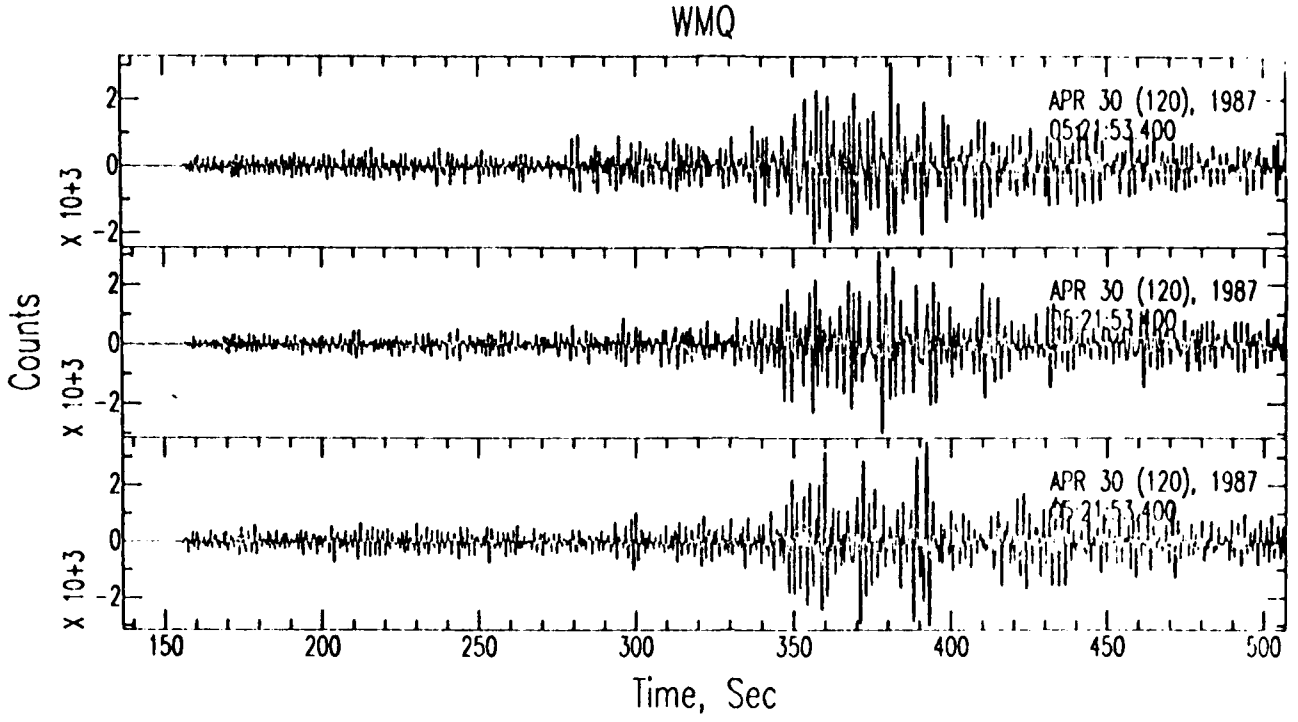

Figure 3.7 The events is near the Sino-Soviet border in southern Xinjiang (near the town of Wuqia). The is a shallow event. The seismograms in Fig. 3.9 are from the same region. They appear quite similar.

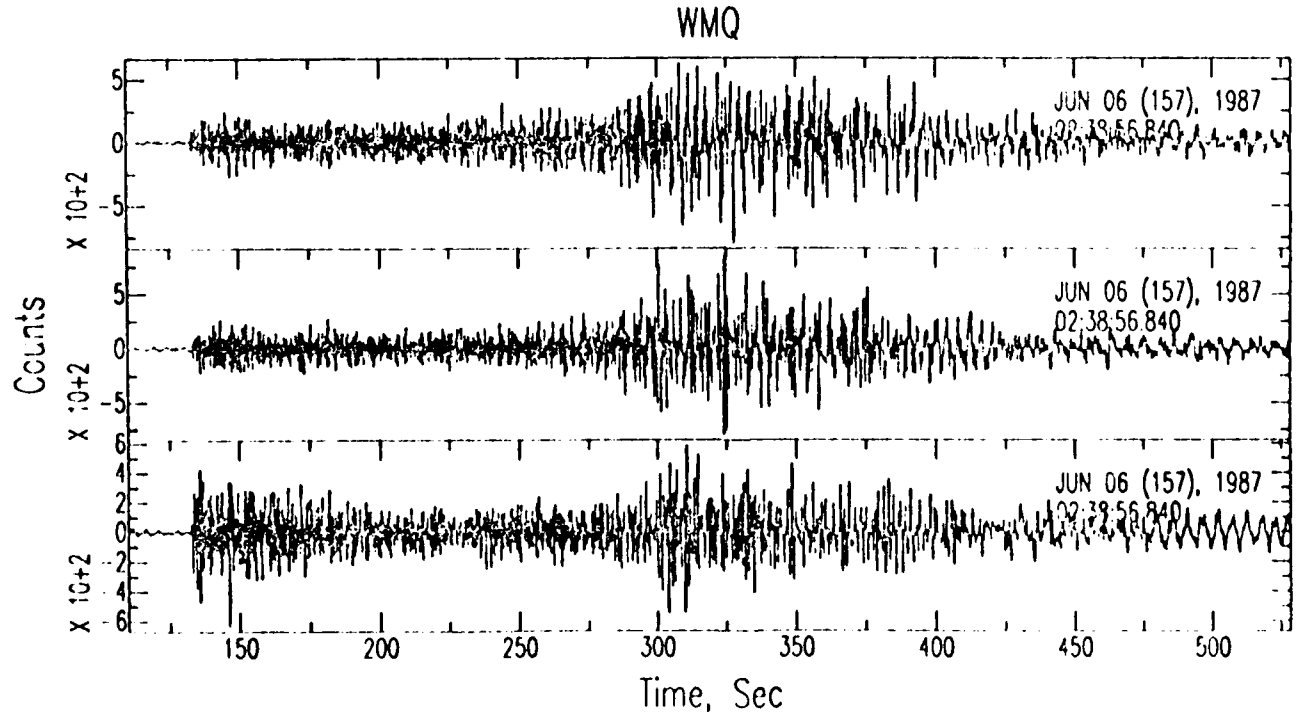

Figure 3.8 This is an Semipalatinsk event (evidently from the Degelen site, judging from the epicentral location and waveform - see more later). The Lg velocity for the first group is 3.4 km/sec. Compare Figure 3.10 and notice the overall difference between this figure and the Shagan River event records (Figure 3.10). (Pn/Lg)z for Shagan River events are consistently larger than those for the Degelen events. A characteristic large phase at about 15 seconds after the Pn is clearly observed in all cases for the Shagan River events, but not usually for the Degelen events. See next section for detailed comparison of P waves for these two groups of events. The short period (~5 seconds) surface waves train are very different for these events. But unfortunately the triggered records do not usually include the later waves.

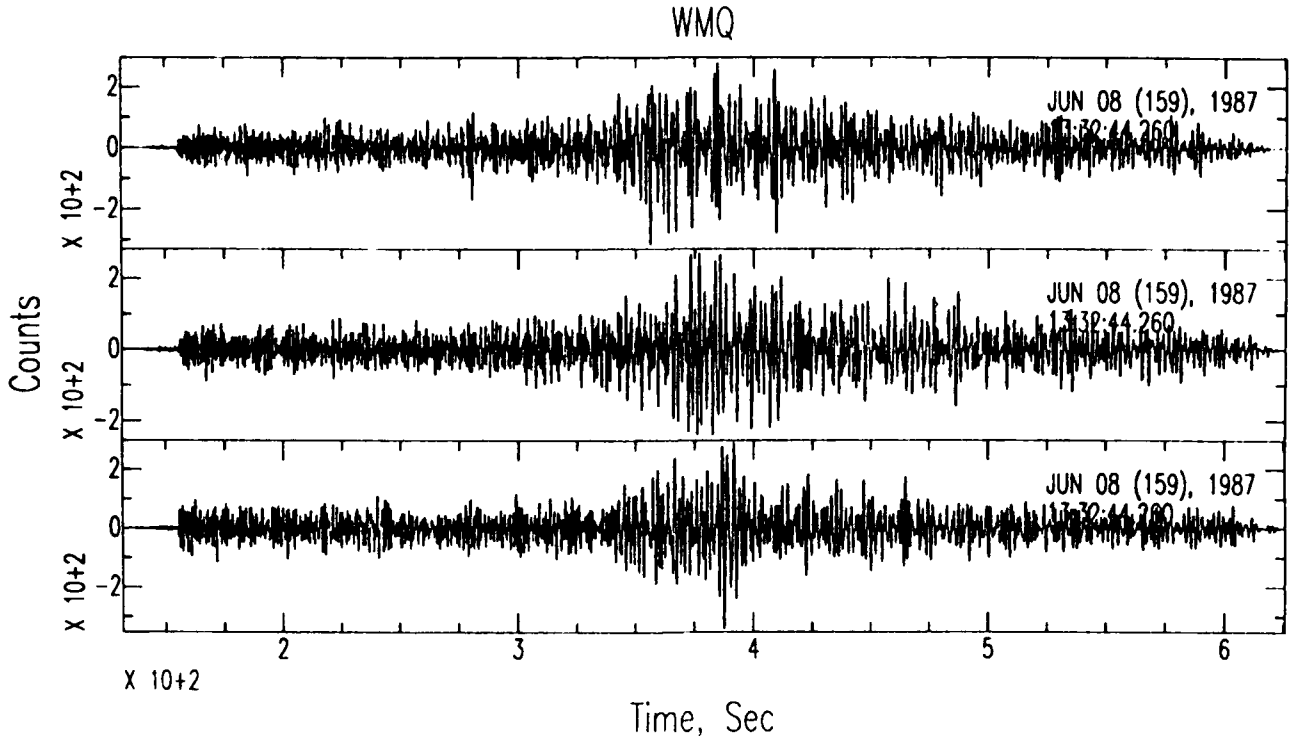

Figure 3.9 The events is near the Sino-Soviet border and at the east terminus of the Pamir mountians. The is a shallow event. The Lg phase arrives with a velocity of 3.44 km/sec.

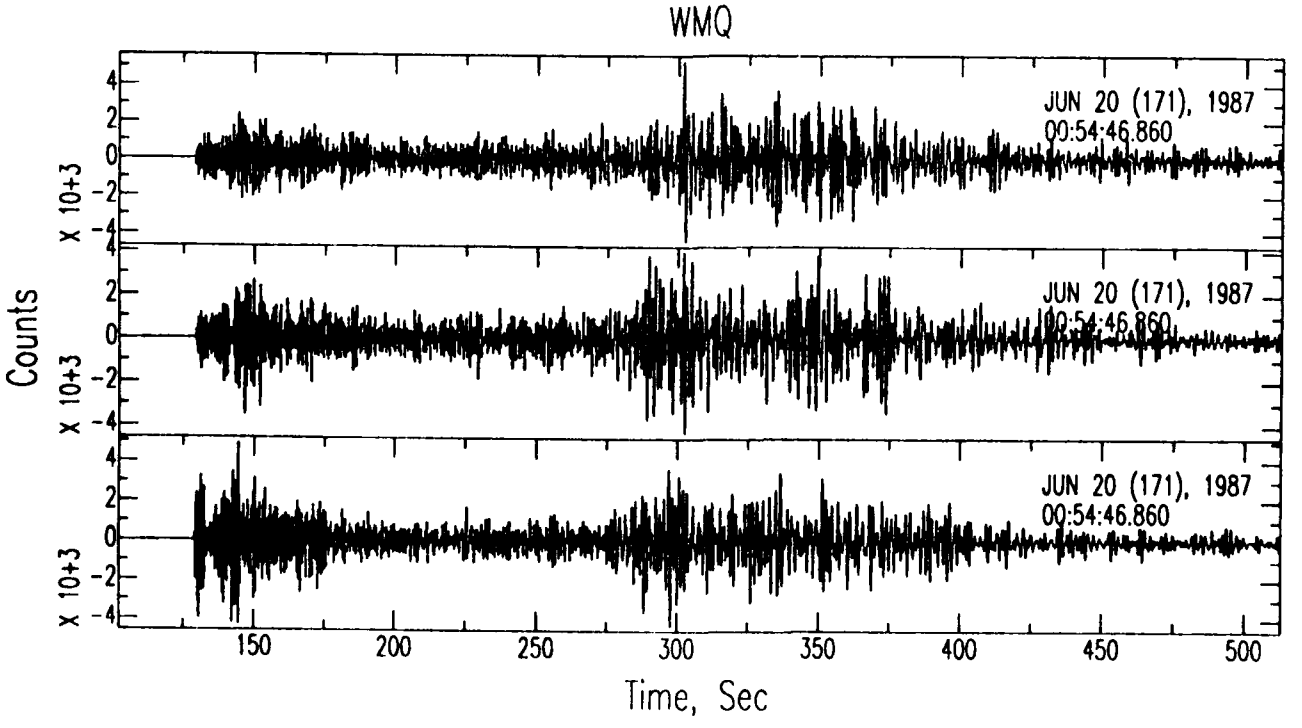

Figure 3.10 See figure caption for 3.8.

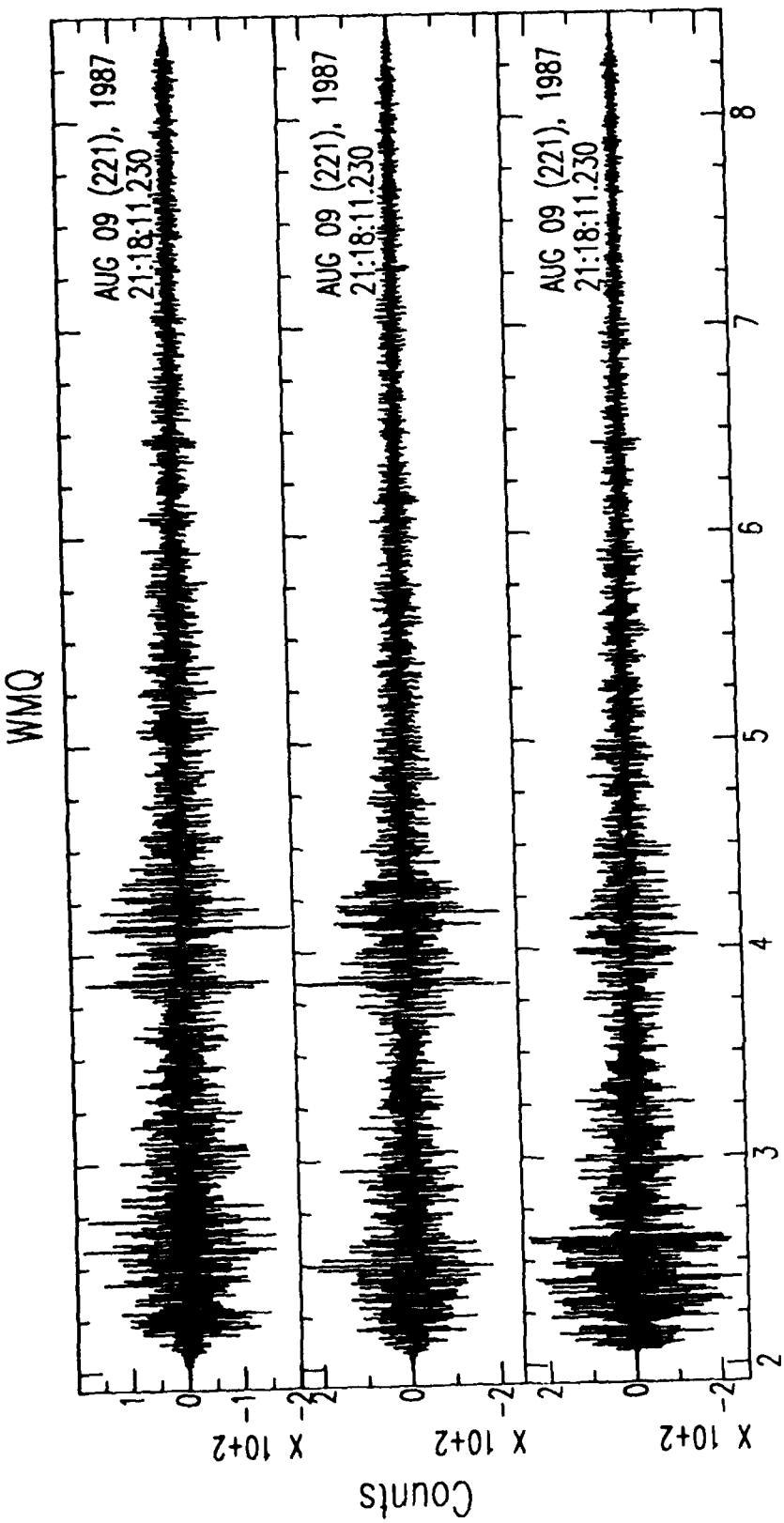

Figure 3.11 This event is located in the western Himalayas. Notice the relatively large P waves and the absence of Lg waves (3.4 km/sec arrival is expected at about 450 seconds). This observation is consistent with previous observations of Ni and Barazangi (). The apparent velocity of the P wave is 7.94 km/sec.

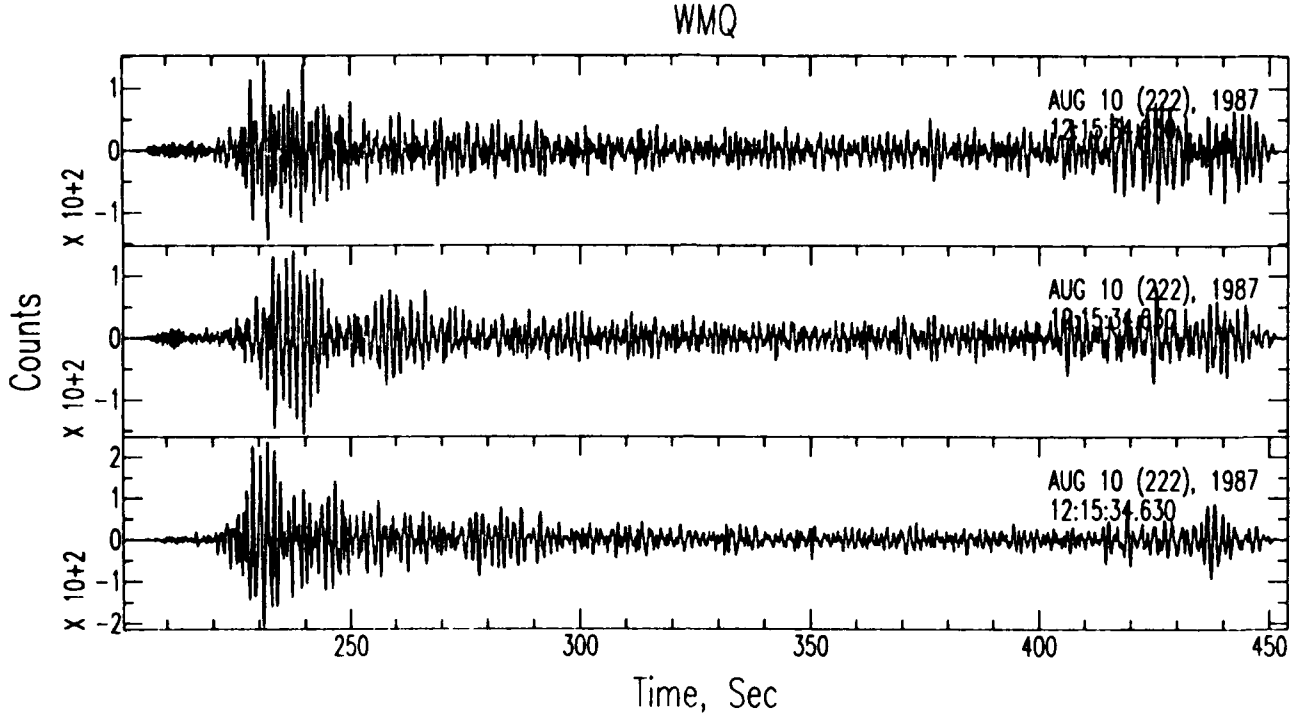

Figure 3.12 This event is located at the western edge of the Ordos Platform in the vicinity of the Yingchuan Graben. The (a) WMQ and (b) LZH records are shown here. At LZH, the closer station, the Lg arrives with a velcity of 3.57 km/sec; at WMQ the triggered records stopped short of the Lg wave.

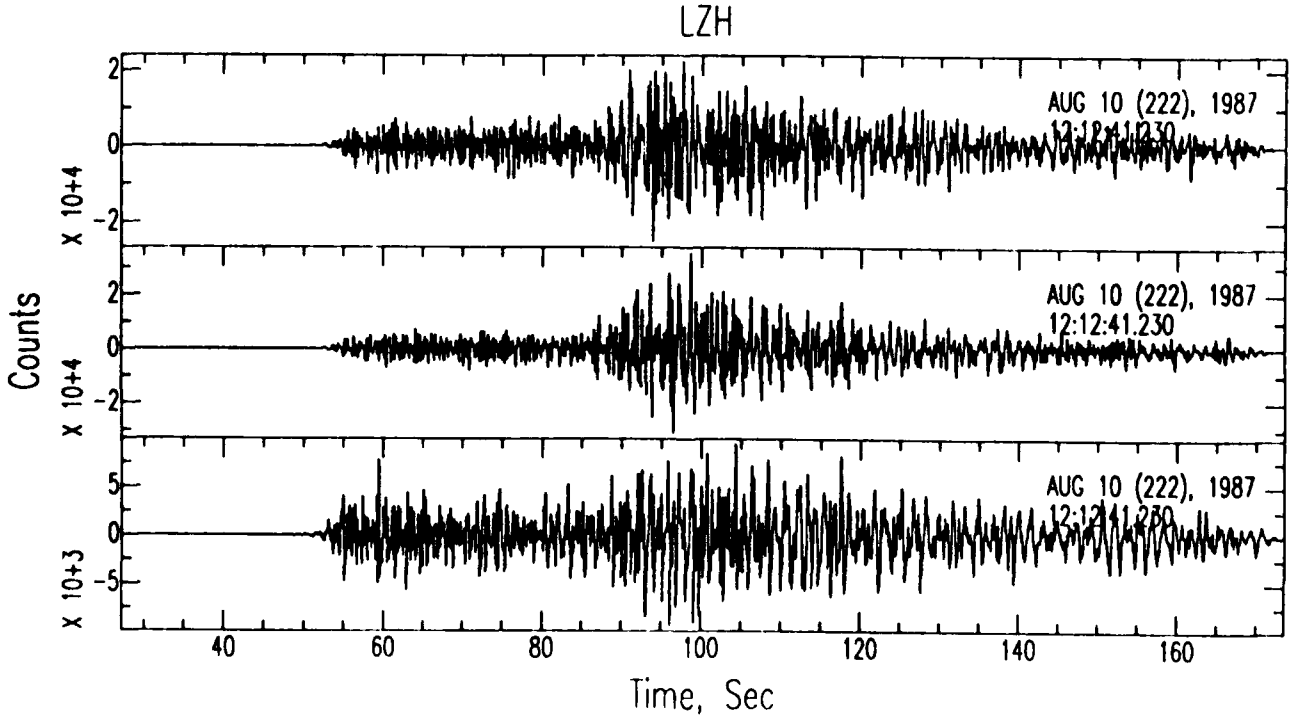

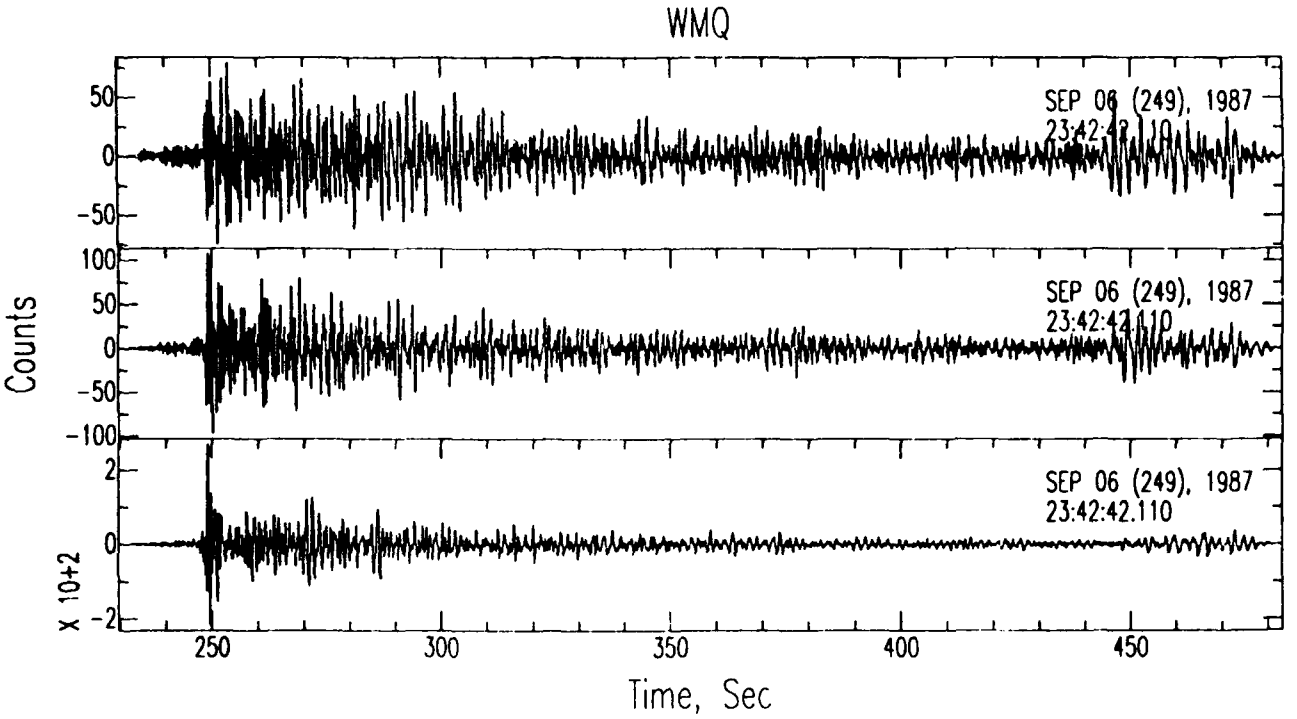

Figure 3.13 An event from the eastern Himalayas. (a) WMQ and (b) KMI records are shown. The path to KMI is contained almost entirely within the southern edge of the Tibetan Platean, much in the Himalayas. The records show evidence of scattering. No trace of Lg can be found in the KMI record (expected arount 280 seconds.

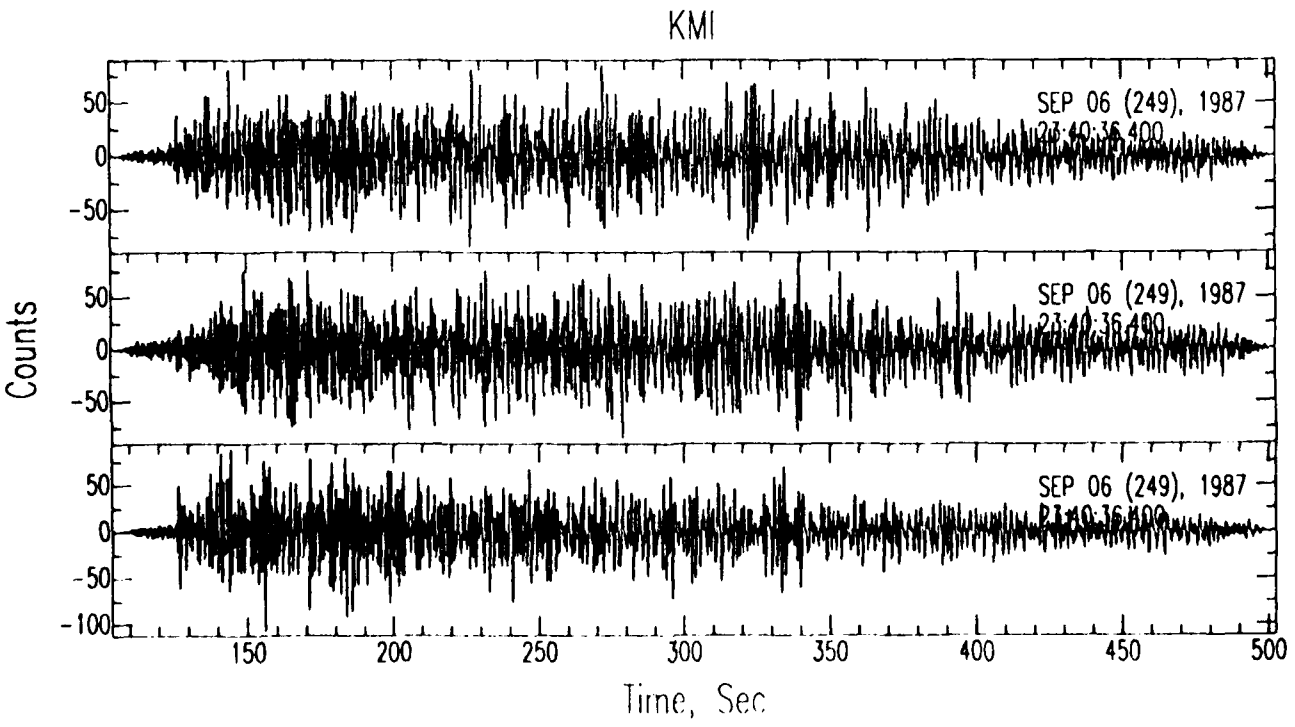

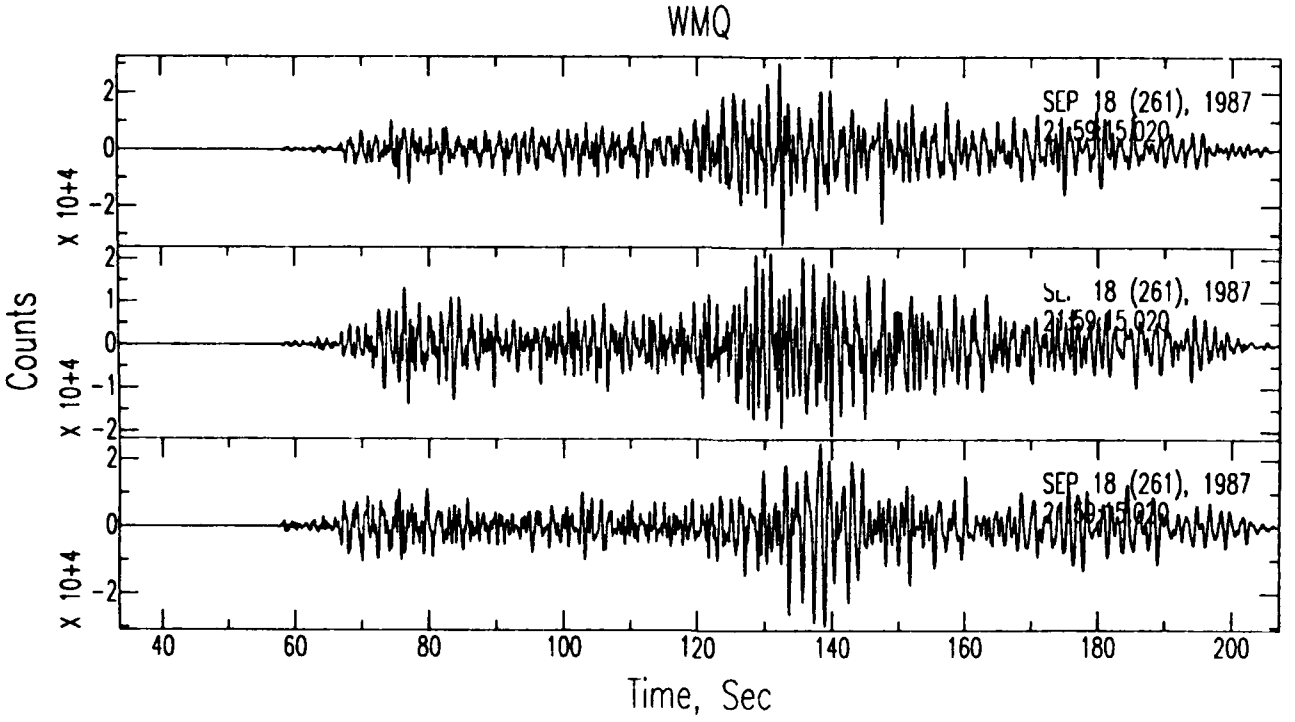

Figure 3.14 An event in the Altai mountains east of the Zhungar Basin.

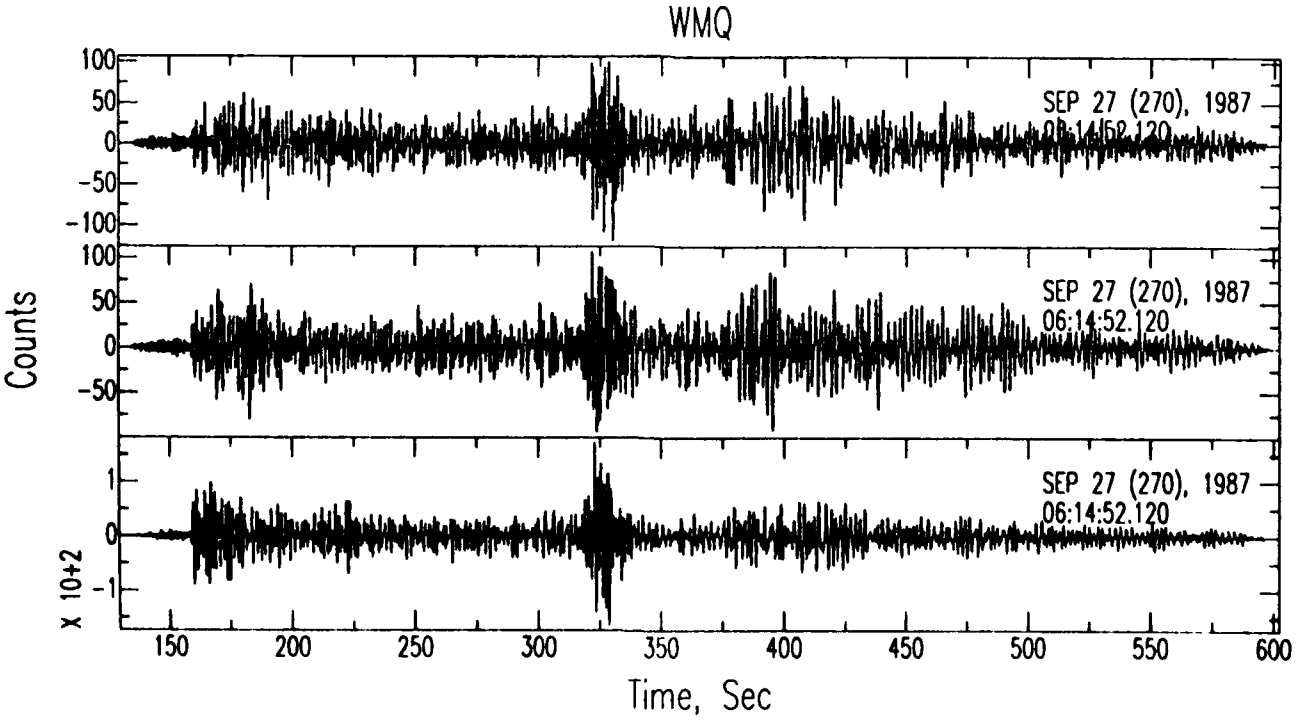

Figure 3.15 An event in northwestern Tibet near the Karakunruns. The Lg appears as a small but visible phase with a velocity of 3.3 km/sec. A burst of energy at 325 seconds represents probably a local shock.

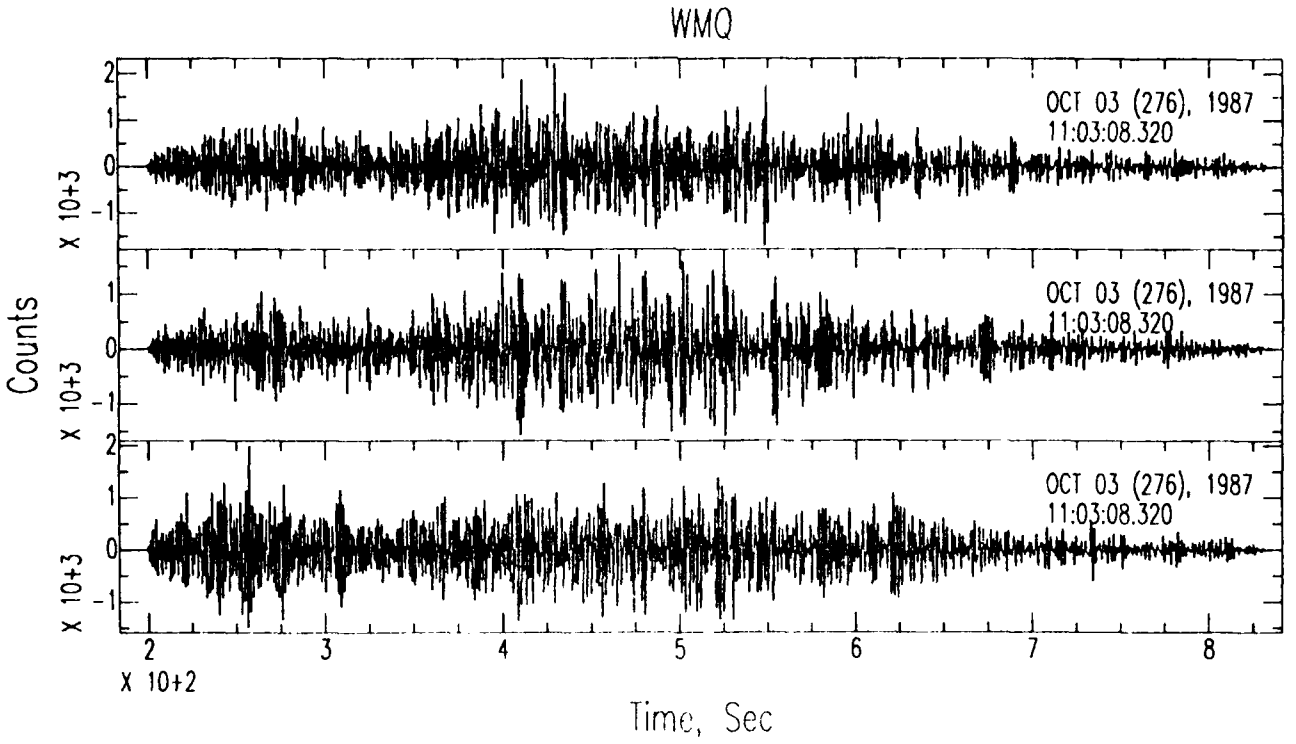

Figure 3.16 An intermediate shock from the Pamirs recorded at WMQ. Here a large P wave is seen, but no Lg can be found.

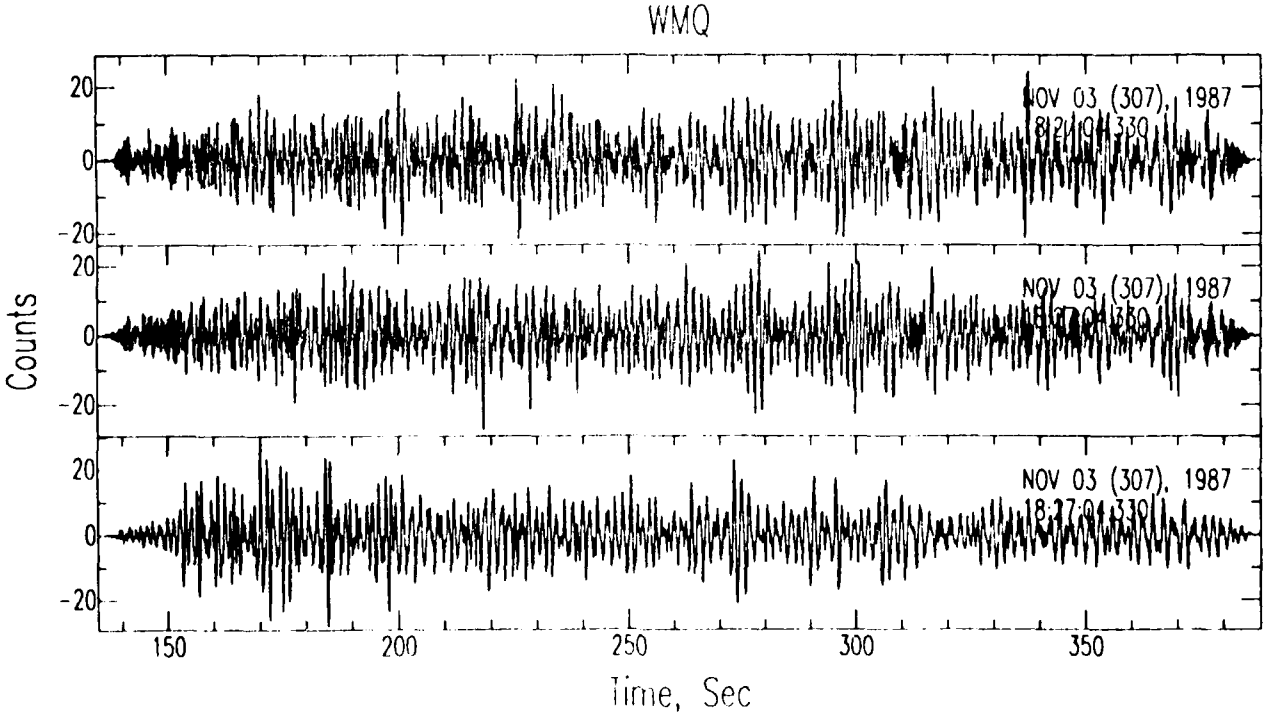

Figure 3.17 An event in the central western part of the Tibetan Plateau recorded at WMQ. Scattered waves dominate the seismograms. No Lg phase (expected to arrive at 350 seconds) can be seen.

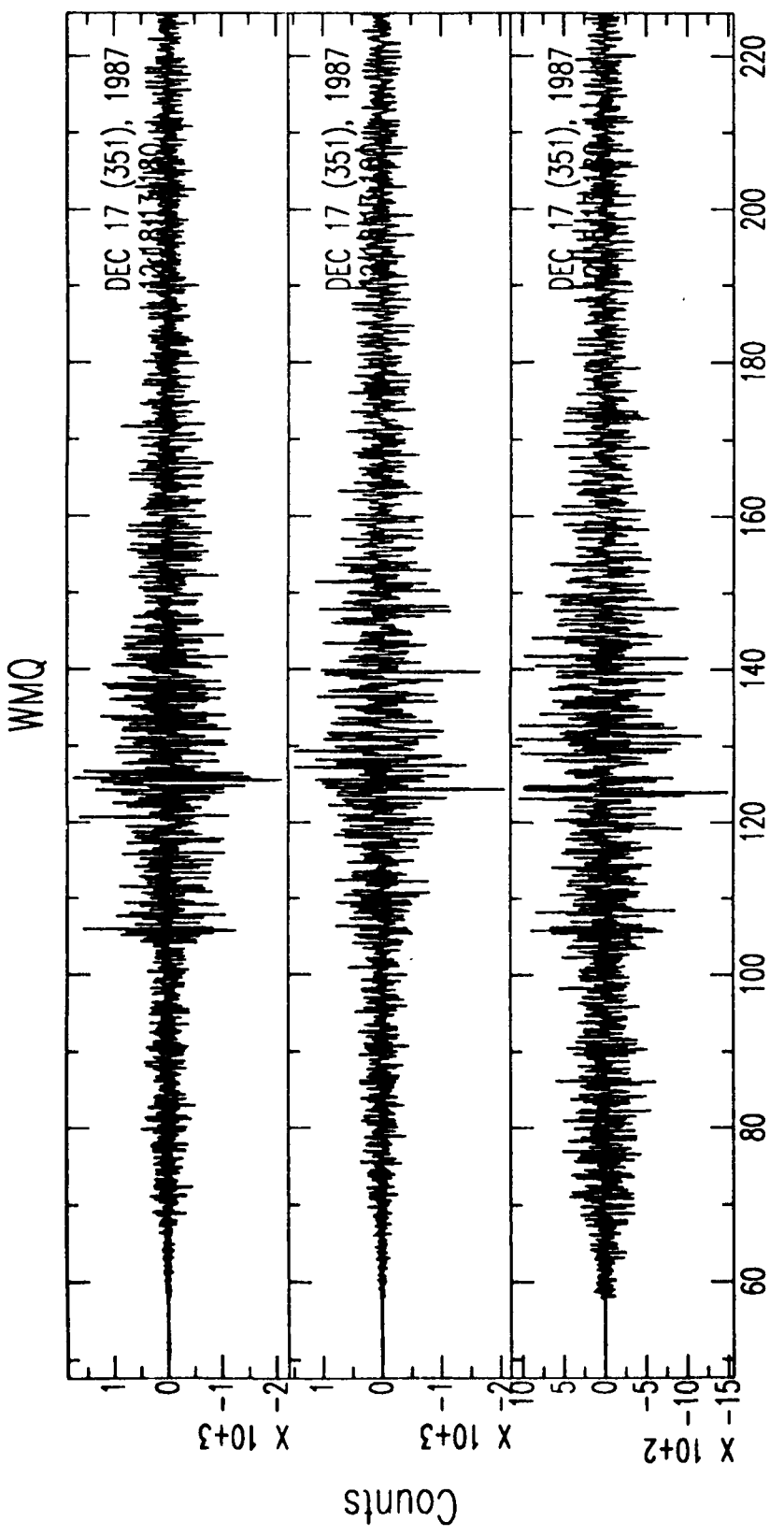

Figure 3.18 These and the next set of records are from events in the southern Tianshan, north of the Tarim Basin.

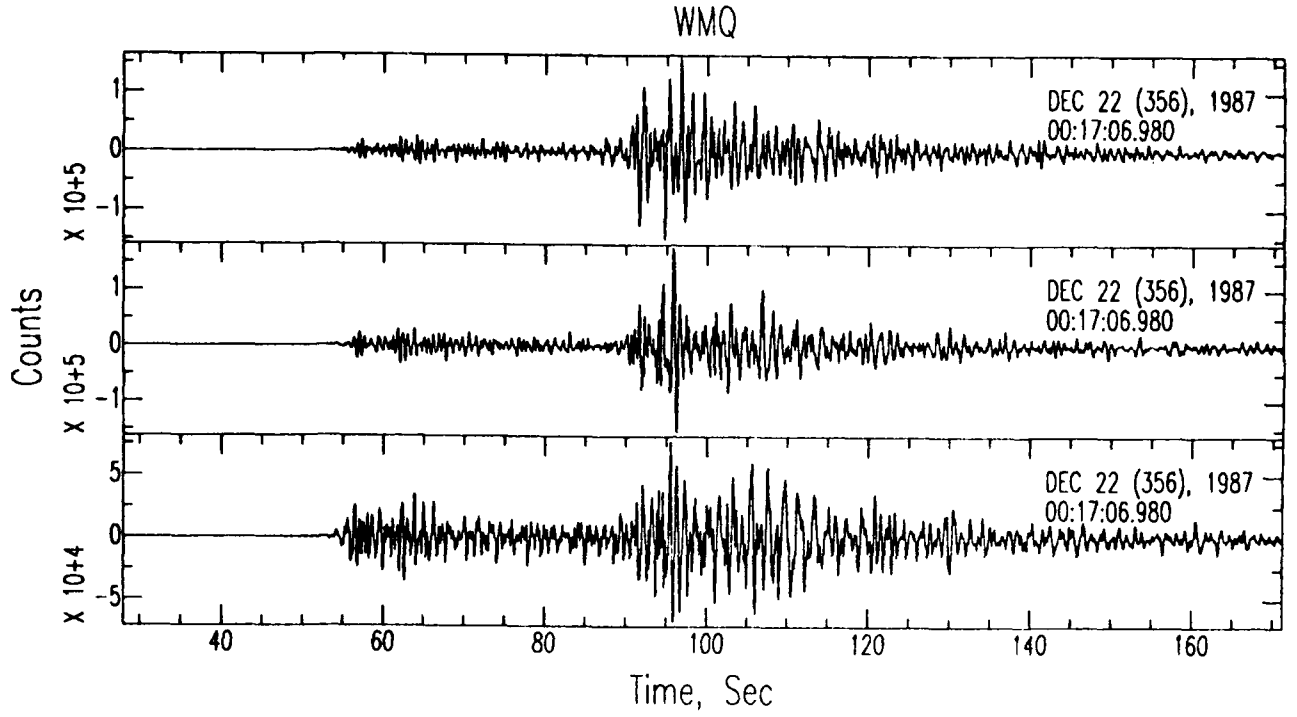

Figure 3.19 See caption for Fig. 3.18.

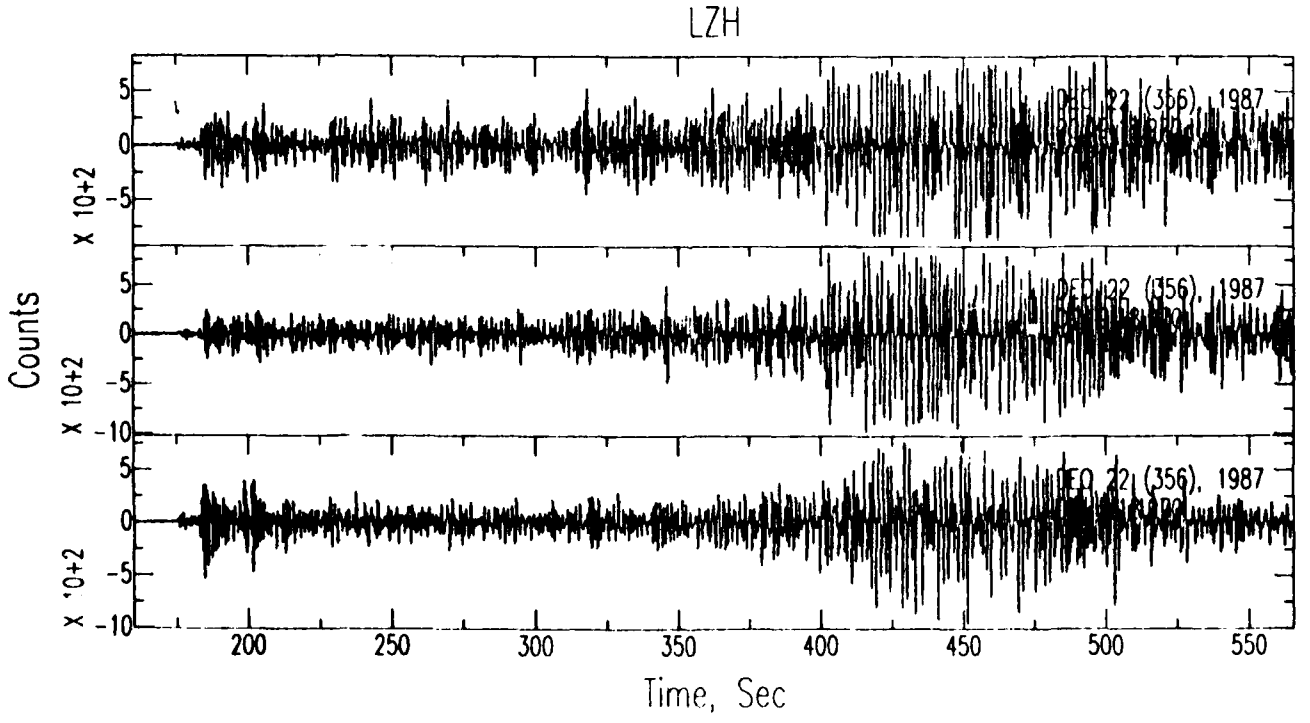

4 Observations of events from Semipalatinsk

Seismograms of the Semipalatink events at CDSN stations are interesting, and not yet completely understood. As expected, the events in the eastern part of the test site (Shagan River) produce seismograms that are quite distinct from those for events in the western part of the test site (Degelen Mountains). The events are listed in Table 4.1.

Table 4.1 Information for Semipalatinsk events

Julian Day	Lat.	Long.	Date	O. Time	M_b	M_s
87071	49.94	78.82	03-12	01:57:17.2	5.5	3.9
87093	49.93	78.83	04-03	01:17:08.0	6.2	4.7
87107	49.89	78.69	04-17	01:03:04.8	6.0	4.3
87126	49.83	78.13	05-06	04:02:05.6	5.3	
87171	49.91	78.73	06-20	00:53:04.8	6.1	4.2
87198	49.78	78.13	07-17	01:17:07.0	5.8	4.6
87214	49.84	78.89	08-02	00:58:06.7	5.9	3.8
87319	49.87	78.79	11-15	03:31:06.7	6.0	4.8
87347	49.96	78.85	12-13	03:21:04.7	6.1	4.5
87354	49.83	78.00	12-20	02:55:06.7	4.8	
87361	49.83	78.74	12-27	03:05:04.7	6.1	4.5

4.1 Seismograms for the Shagan River and the Degelen Sites Recorded at WMQ, LZH and BJI.

The epicentral distances of WMQ, LZH and BJI stations to the Soviet test sites are around 8.8, 23 and 31 degrees, respectively. While the first arrival at WMQ is P_n, the P waves arrive at LZH and BJI have travelled through upper mantle. Detailed interpretation of the P phases in all three cases would be difficult. However, comparison of the initial P waves and phases arriving within 20 seconds of the initial P, demonstrate great differences of the seismograms from the Shagan and Degelen sites as well as subtle difference among the individual events at either site. These records have been shifted in time to align either at the first arrival or the maximum (or minimum) of the first cycle.

As we can see from Figs. 4.1.1 through 4.1.4, SPZ seimograms for the Shagan and Degelen events recorded at WMQ, the initial P at WMQ are much more impulsive for the Shagan than for the Degelen events. The initial motion of the Degelen records can best be described as emergent. Incidentally, the broad-band IPZ records show sharper P first arrivals, but the overall waveforms are quite similar and we have more SPZ records available for comparison. On the Shagan River records a large phase at about 3 seconds after the initial P can be observed, but it is virtually absent in the Degelen records. Another characteristic phase in the Shagan records are the prominent five cycles at about 14

seconds after the initial P. This phase appear as one and half cycle phase for the Degelen events and arriving slightly later. For both the Shagan and the Degelen records, the pP phases can be clearly discerned (Fig. 4.1.1), based on comparisons with studies of Burdick et al. (1989).

A detailed interpretation of these phases is difficult. By comparing the similarities and differences of the Degelen and Shagan events recorded at WMQ we make the following observations:

(1) It is quite remarkable that two sites that are less than 70 km apart can generate regional waveforms that are clearly different.

(2) Based on its variability, and the absence of it for the Degelen records, the phase at 3 seconds or so after the initial arrival is probably a wavetrain associated with velocity structures near the source.

(3) The phase at 15 or so seconds after the initial break for both Shagan and Degelen events are probably a phase having a common path, but a part of the phase is probably associated with a up-going ray near the source, causing the differences observed between the Shagan and Degelen records.

(4) Detailed study of these waveforms with synthetics will be quite interesting.

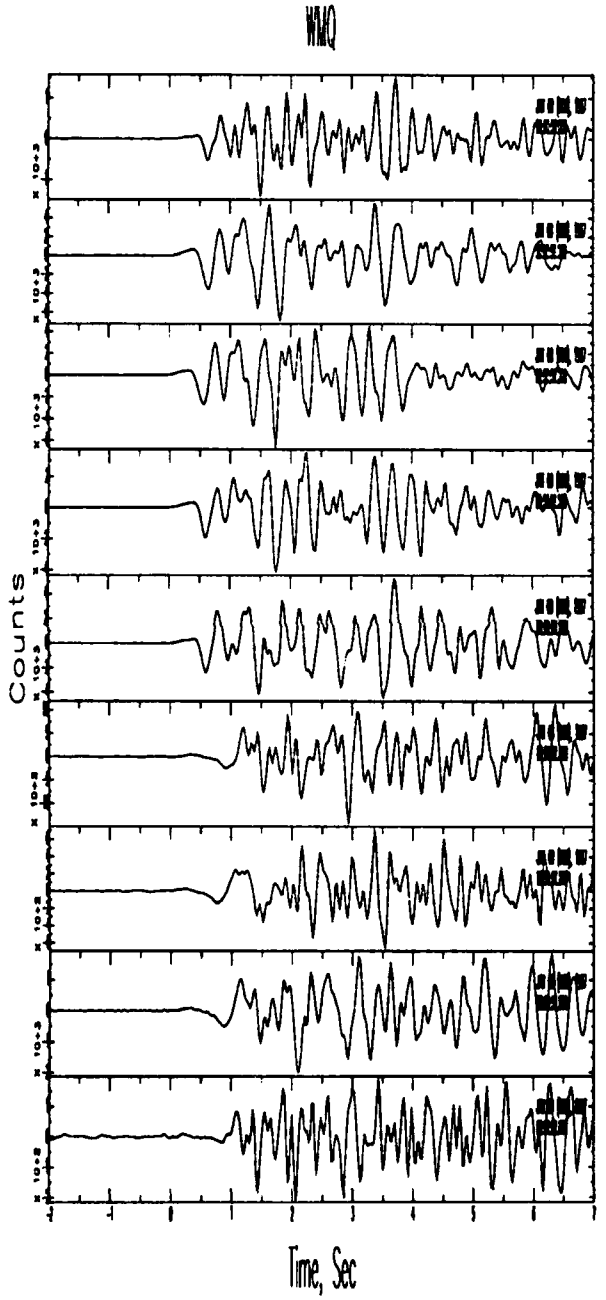

Fig. 4.1.1. The first seven seconds of the SPZ records of 1987 Shagan and Degelen events recorded at WMQ. The details of P waves are shown here. These records are lined up at the first motion. The top five traces are from the Shagan events (corresponding to events numbers 87071, 87093, 87171, 87 214, and 87347) and the lower four are from the Degelen area events 98126, 87157, 87198, 87354). Notice that while first motions for Shagan events are clearly up, those for the Degelen events are emergent when plotted at this scale. By increasing the vertical scale we can see the upward first motions for both Shagan and Degelen events (Figs. 4.1.3 and 4.2.4). Also, for the Shagan records a clear phase arrives at 3 seconds after the initial break.

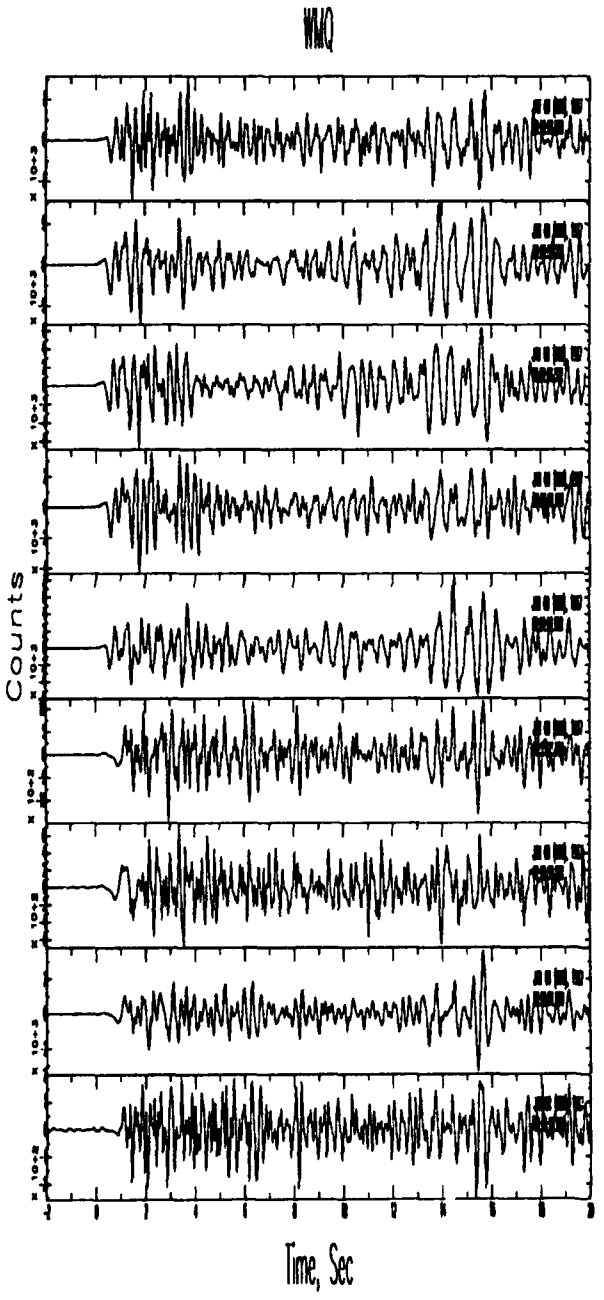

Fig. 4.1.2. The first twenty seconds of the SPZ records of the 1987 Shagan and Degelen events (in the same order as that of Fig. 4.1.1) recorded at WMQ. Clearly displayed are the arrivals for both Shagan and Degelen events at 14 to 15 seconds after the initial breaks. The detailed waveforms of this phase for the Shagan and Degelen events are significantly different. Notice that the overall differences in the waveforms of these two groups of records are also quite clear.

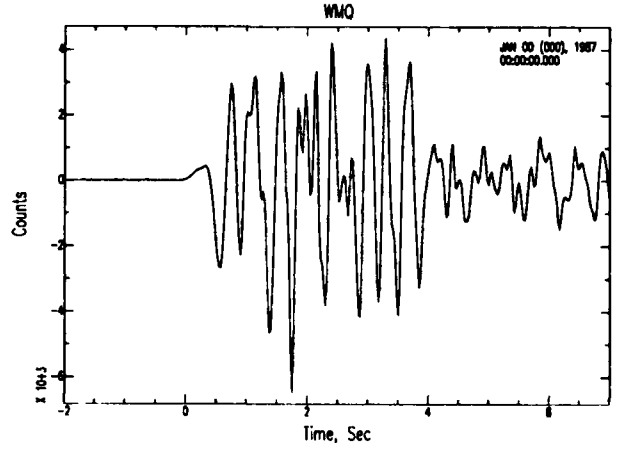

Fig. 4.1.3. Details of SPZ records of Shagan River event 87171 recorded at WMQ. Notice the clear first motion and the differences between this record and Fig. 4.1.4.

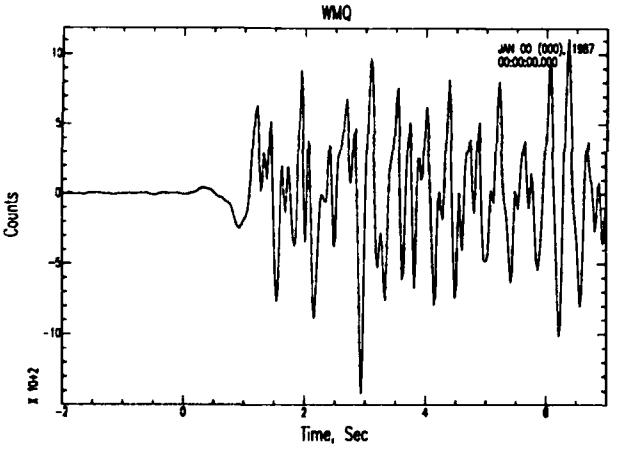

Fig. 4.1.4. Details of SPZ records of Degelen event 87126 recorded at WMQ.

Fig. 4.1.5 presents the records of the Shagan River and Degelen events recorded at BJI. The epicentral distance is about 28 degrees. The pP phase is not very clear as shown in the LZH records (Fig. 4.1.6).

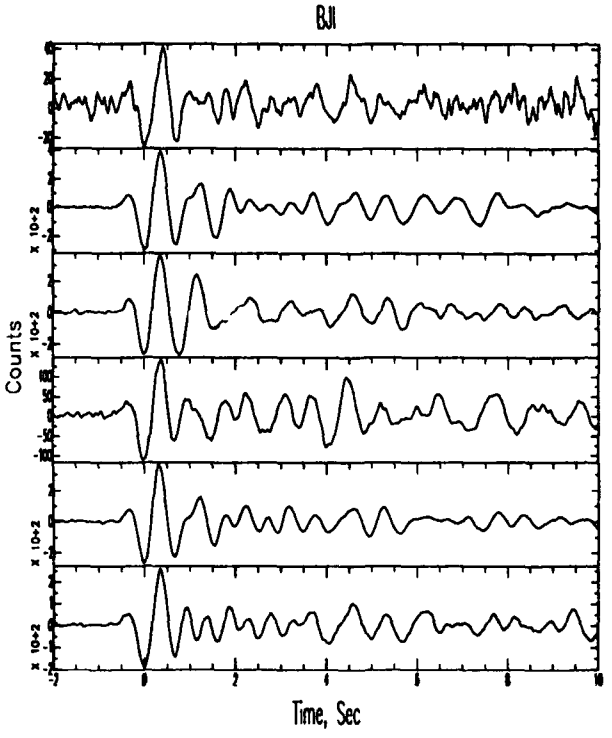

Fig. 4.1.5. SPZ records of Shagan River and Degelen events recorded at BJI. The records from events (from top)
87071
87093
87107
87214
87319
87347
87126 (Degelen)
Notice the very noticeable differences between the Shagan River and Degelen records.

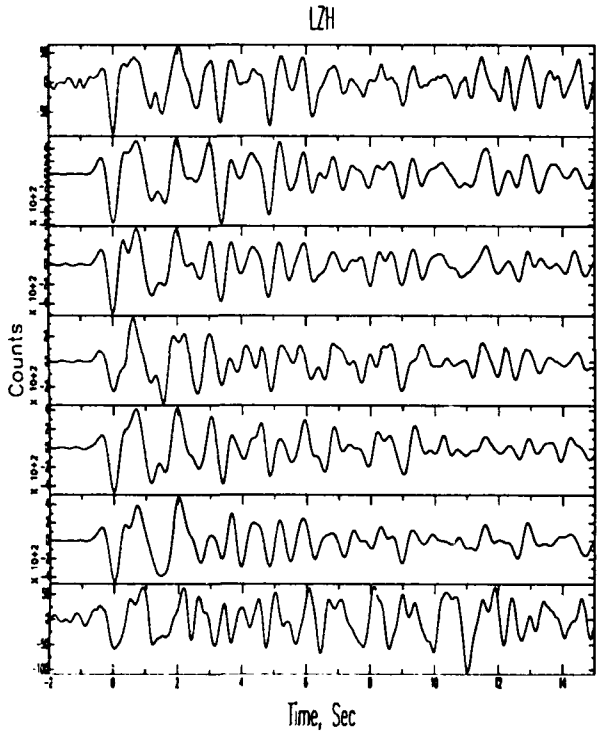

Fig. 4.1.6. SPZ records of Shagan River and one Degelen event recorded at LZH. The events are
87071
87093
87171
87214
87319
87347
87198 (Degelen)

4.2 Cross-correlation of waveforms from different shots

To show the similarities and differences of the Semipalatinsk events, we have performed correlation studies of these events at LZH.

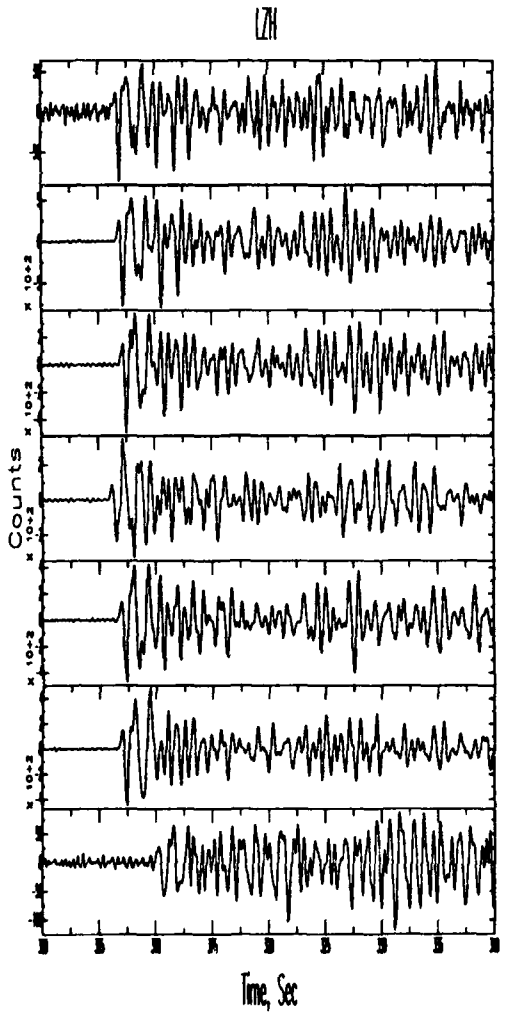

Fig. 4.2.1 SPZ records at LZH.

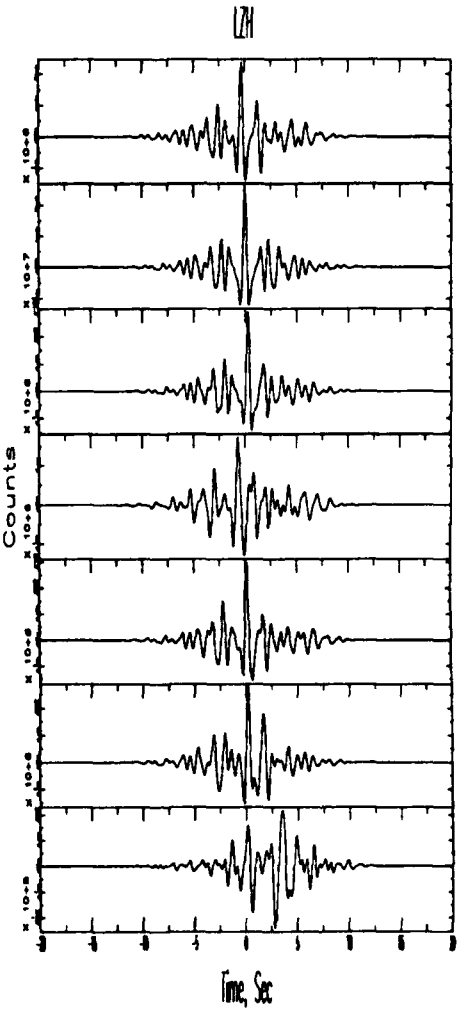

Fig. 4.2.2 Cross-correlation of the records at left.

4.3 Spectral comparison of Shagan events of different sizes

Sample velocity spectra for Shagan events are shown in figures 4.3.1-4.3.6; in all cases a time window of ten seconds is used. For the WMQ spectra, the common features in the spectra are a relative low between 4 and 5 Hz and the high frequency fall-offs are quite similar. While the spectra of event 87071 (Fig. 4.3.1, Mb=5.5) and 87214 (Fig. 4.3.3, Mb=5.9) have similar overall shape, the spectrum for event 87093(Fig. 4.3.2, Mb=6.2) shows clear low frequency enrichment in comparison.

The LZH spectra show however significant low frequency enrichment for events 87071, 87093 and 87214 in comparison to the WMQ records of the corresponding events. The flattening of the LZH spectra at the high frequency end is evidently ground noise.

The WMQ records show a corner frequency of about 6-7 Hz and the LZH records, on the other hand, has a corner around 1 Hz. The differences evidently arise from the fact that WMQ P waves are composed mainly of crustal phases while the LZH P (and other body) waves have suffered from its double passage through the low-velocity/attenuation zone in the uppermost mantle.

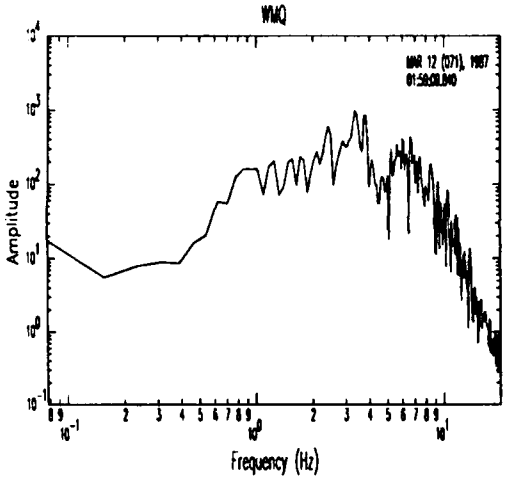

Fig. 4.3.1 Fourier spectrum of the vertical component of WMQ records for event 87071. The corner frequency is at 6-7 Hz.

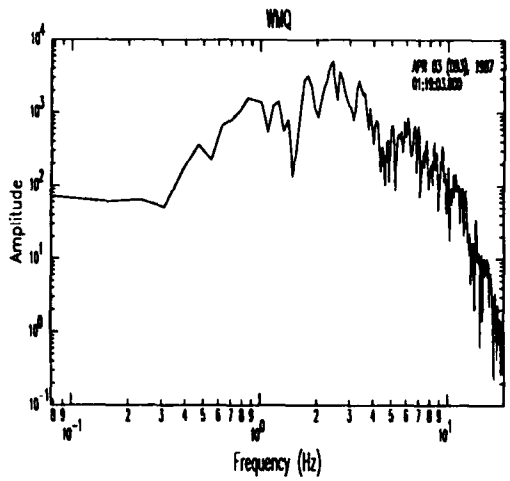

Fig. 4.3.2 Fourier spectrum of the vertical component of WMQ records for event 87093. Although the long period content is enriched compared to the spectrum in Fig. 4.3.1, the corner frequency is still at 6-7 Hz.

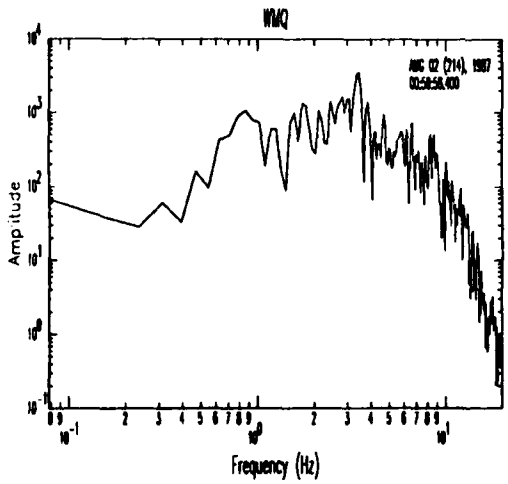

Fig. 4.3.3 Fourier spectrum of the vertical component of WMQ records for event 87214. The enrichment of low frequency compared to the spectrum in Fig. 4.3.1 is clear.

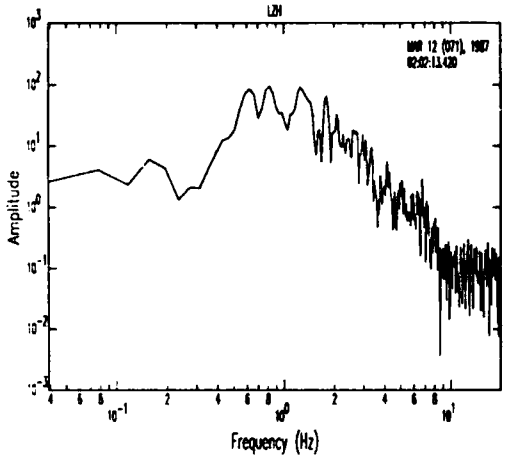

Fig. 4.3.4 Fourier spectrum of the vertical component of LZH records for event 87071. The corner frequency is at 1-2 Hz and noise dominates the spectrum beyond 8-9 Hz.

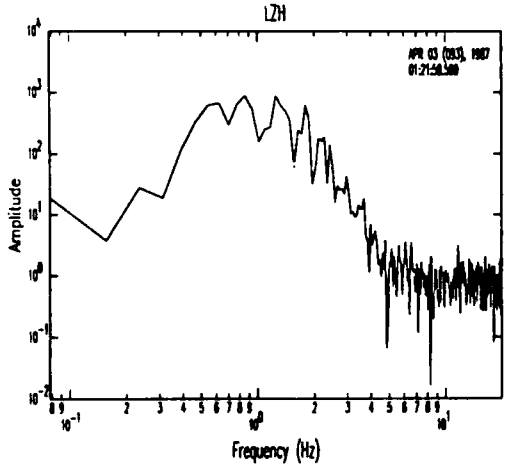

Fig. 4.3.5 Fourier spectrum of the vertical component of LZH records for event 87093. The corner frequency is at 1-2 Hz. The noise dominates beyond about 5 Hz.

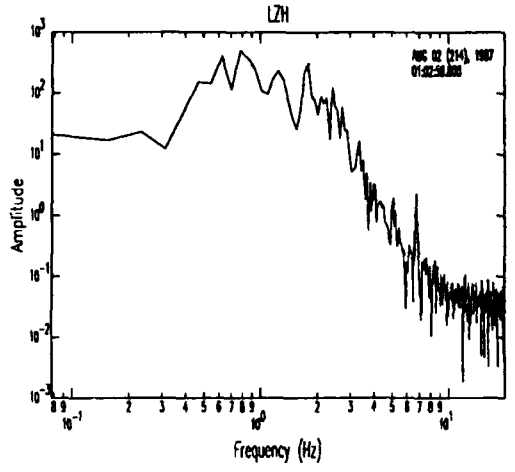

Fig. 4.3.6 Fourier spectrum of the vertical component of LZH records for event 87214. The corner frequency is at 1-2 Hz and the noise dominates the spectrum beyond about 8 Hz.

5 Regionalization of Rayleigh and Love Waves using CDSN Seismograms

5.1 Introduction

The purpose of this work is to derive the Rayleigh and Love group velocities appropriate for various geologic/tectonic provinces in China. The results available to-date are based on relatively sparse path coverage over China (e.g., Feng and Teng, 1983). With the established of Chinese Digital Station Network (CDSN), the quality of the available data has increased immensely. Although data from only four to six stations were available to us during 1987 and the first half of 1989, we are able to use many magnitude M_S 4 to 5.5 (as well as a few larger) earthquakes as sources for this work. Events used include continental ones located in Central Asia, western China, the Pamirs etc (Fig. 5.0.1) and a number of them near Japan.

The approach used in this study is to assign regional boundaries and determine the velocities for these regions through an inversion of the measured group travel times of the Rayleigh waves traversing across them. Similar method has been used by many others (e.g. Nishimura and Forsyth, 1988).

5.2 Group Velocity Determination

5.2.1 Program for rapid interactive group velocity determination

We have written an interactive group velocity determine routine on the Sun workstation utilizing SAC (Seismic Analysis Code, LLNL) graphics subroutines. It takes less than two minutes to compute and plot (on the screen) the result of a multiple filter group velocity analysis in the period range of interest. The subsequent determination of group velocities may involve

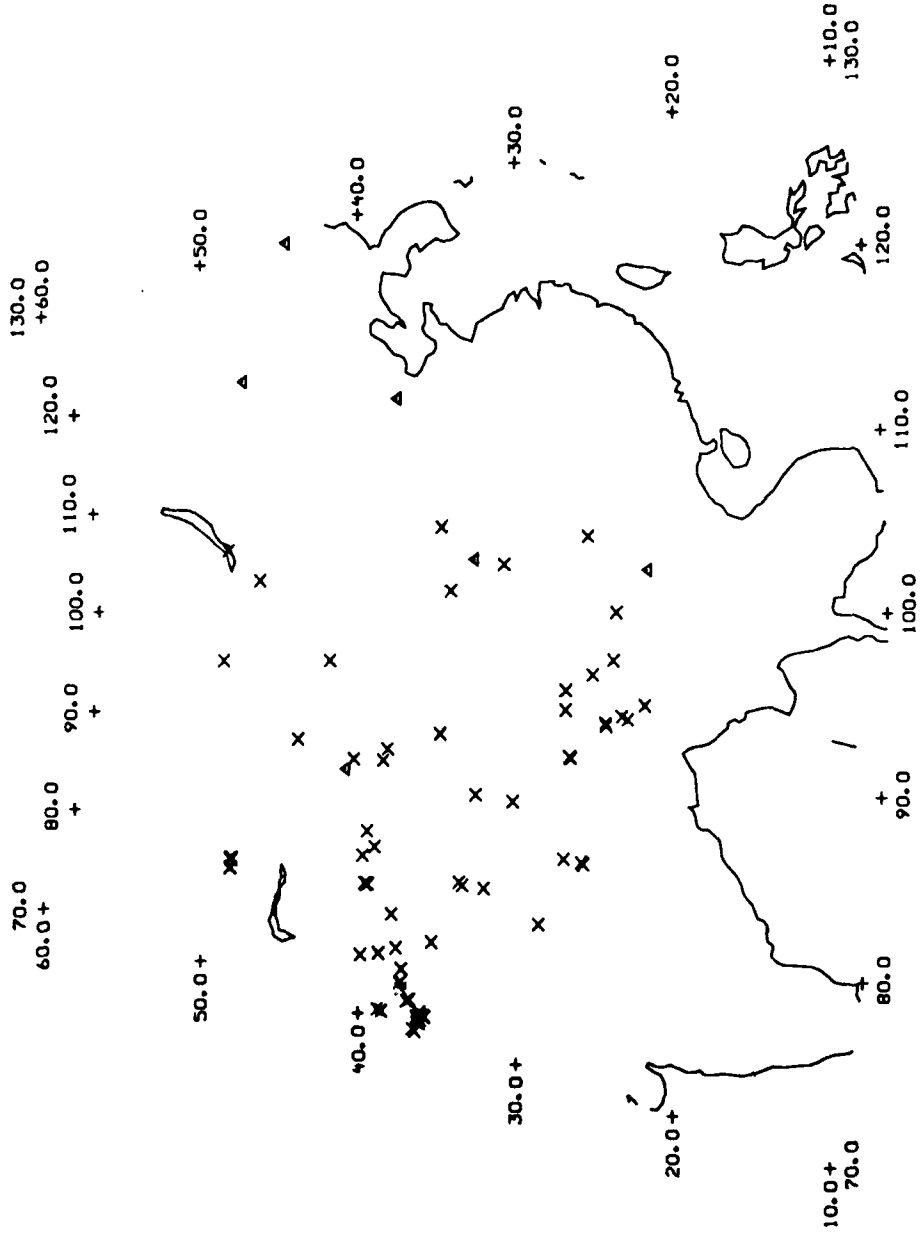

Figure 5.0.1 CDSN stations and the 1987 event locations.

ambiguities because of the presence of higher modes, the arrival of later surface waves due to lateral refraction or even body waves. In such cases human intervention is needed to locate the secondary maxima, rather than the absolute maxima, on the energy envelop. We have developed an interactive routine in which a point on the curve is adopted if no stepwise change in group velocity occurs, otherwise a secondary maximum will be sought by the program until it satisfies the user. This procedure evidently involves subjective judgment and some experience on the part of the user is therefore needed. The resulting group velocity vs frequency is stored in a file for further processing.

5.2.2 Data

An event search at the Center for Seismic Studies was performed to include all 1987 m_b>4.8 events within the latitude range of 25°*N* and 60°*N* and the longitude range of 70°*E* and 120°*E* and data from the CDSN stations (Fig. 5.0.1) were extracted from the archive tapes. Data tapes were written at IRIS. They include the explosion events in the Semipalatinsk test sites, and earthquakes in the Lake Baikal area, in western China, in the Pamirs etc. This dataset is augmented by first half of the 1989 data, obtained through IRIS Data Management Center in Austin Texas. This later set includes more events from Japan Arc area, intended for use to cover some holes left by the first dataset. The files were converted to SAC (Seismic Analysis Code) format and processed on the Sun workstation. Fig. 5.0.1 shows the events used. As shown in Fig. 5.2.1, the ray paths criss-cross a large portion of China. It is already clear however that some blocks are still under-sampled. Some events in the Ryukyus and Taiwan area in the next few years should allow us to have enough data for the area of interest.

Because the wide dynamic range of the digital data, we have been successful in using events with m_b 4.8 (some with M_S as low as 3.9) or higher for surface wave dispersion in the period range of about 15 to 70 seconds. Fig. 5.2.2 shows two example of the contour plot and the group velocities determined; the June 8, 1988 M_S 4.3 event produced excellent result. In fact, some of the low magnitude events gave clearer dispersion than larger events presumably due to the complexity of the sources of the larger events. Explosions invariably yield consistent and well defined group velocities. The dataset was carefully checked and about 15% of the curves were abandoned because of incomprehensible dispersion patterns.

5.3 Geologic and Tectonic Regionalization

The crust in the area of investigation is very complex, with blocks of diverse geologic characteristics juxtaposed as a result of successive collisions in the geological past. As a first effort we have regionalized China guided by the geologic map of China. Units with distinctive petrology (e.g.

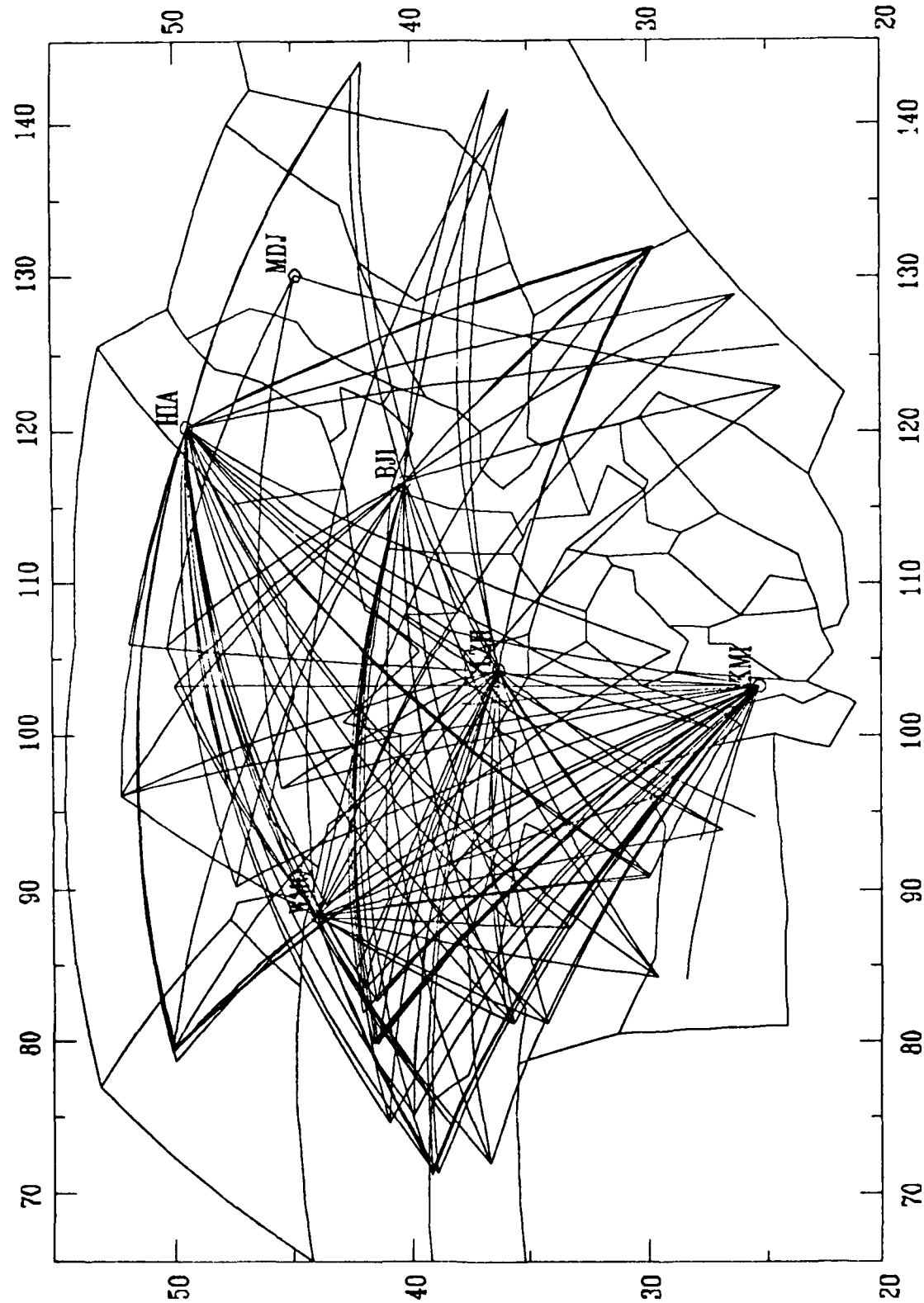

Figure 5.2.1 Ray paths for event station pairs including events in both the 1987 and 1989 sets.

Mesozoic magmatic province of SE China), and of diverse geologic age (e.g. PreCambrian sedimentary rocks south of the Yantze River) and tectonic provinces (e.g. Tibetan Plateau) are classified as different blocks (Fig. 5.1.1), since we may expect them to have different subsurface velocity structures. As shown later, we do not yet have sufficient data to resolve the velocities in all the blocks. We then relax the criteria for subdivision, thus combining various geological provinces shown in Fig. 5.1.1, into larger blocks (Fig. 5.3.1a). We are attempting to find an optimum middle of the way such that the conclusion can be supported by data available now. The soundness of our determinations can be assessed by checking against some "pure path" data. Of course the resolution matrix allows us to assess the quality of the result.

The program for path calculation can accomodate further refinement of regionalization very easily. Experiments are being conducted for regionalization using hexagons of various sizes as well as a simplification of the present scheme. Because many boundaries are more than a few hundred kilometers long, we have used spherical rather than plane geometry for block boundaries. Of course the ray paths are those on a sphere.

5.4 Determination of Regional Group Velocities

The travel time for a group of surface waves, at a particular period, between an event and a station can be written as

$$t_i = \sum_{j=1}^{n} \frac{\Delta x_{ij}}{u_j}$$

where t_i is the arrival time of a group for the ith path, Δx_{ij} is the portion of path through block j and u_j is the group velocity for the j th block. With about 150 paths at this time and the velocities of a total of 25 blocks to be determined, we have a mixed determined problem due to the under-sampling of some blocks. The SVD method is used for the weeding out of the small singular values and the inversion was performed using the decomposition matrices.

5.5 Initial result

Figs. 5.5.1 and 5.5.2 show the results of the initial regression with 1987 data on Rayleigh waves only. In these figures, we have included the regionalized dispersion curves between 20 and 60 seconds as well as the resolution matrix. We have experimented with different cutoffs in the singular values in order to investigate the stability of the solutions. For results shown in Fig. 5.5.1, the cutoff was set at 0.03 of the maximum singular value and for those in Fig. 5.5.2, a cutoff of 0.05 was used.

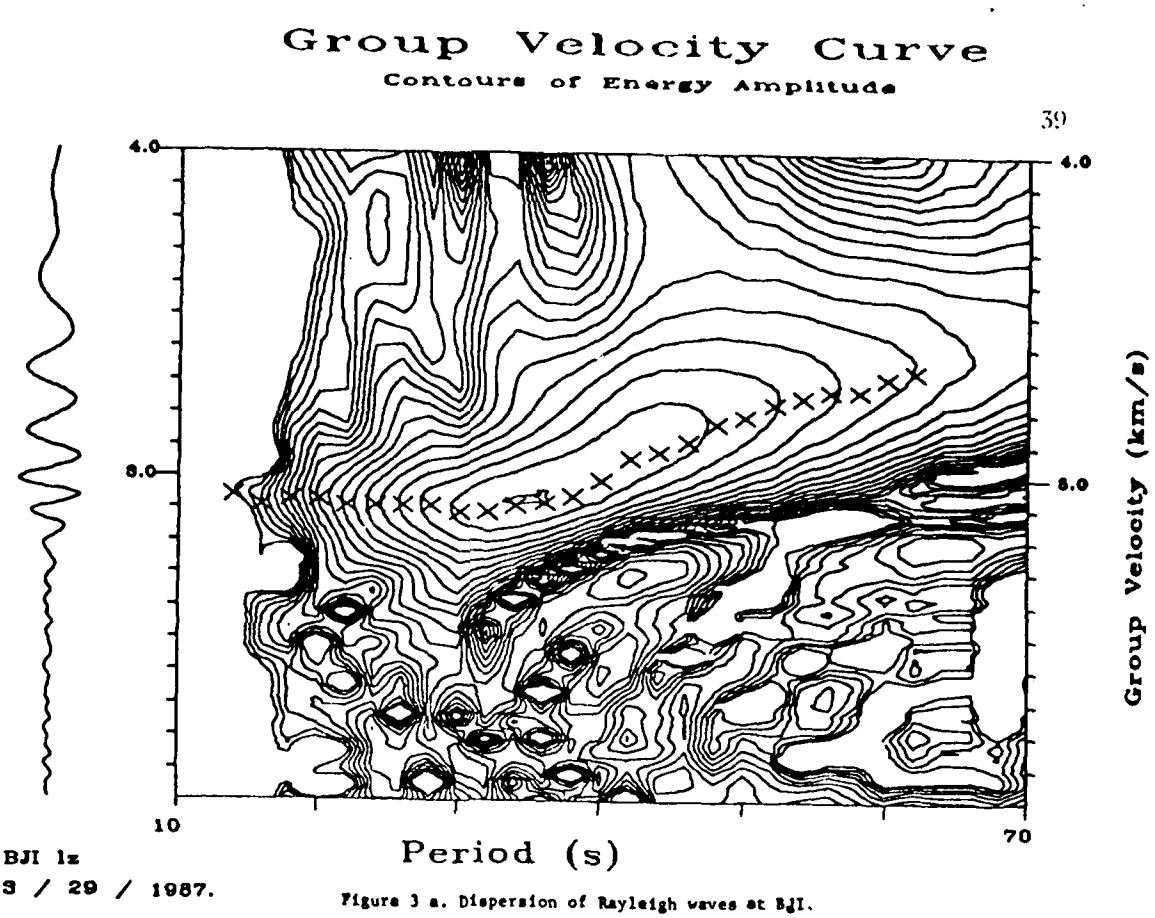

Figure 5.2.2 (a) Raleigh wave dispersion measured at BJI from an event (M_b = 5.0) in Yunnan Province, in southwest China.

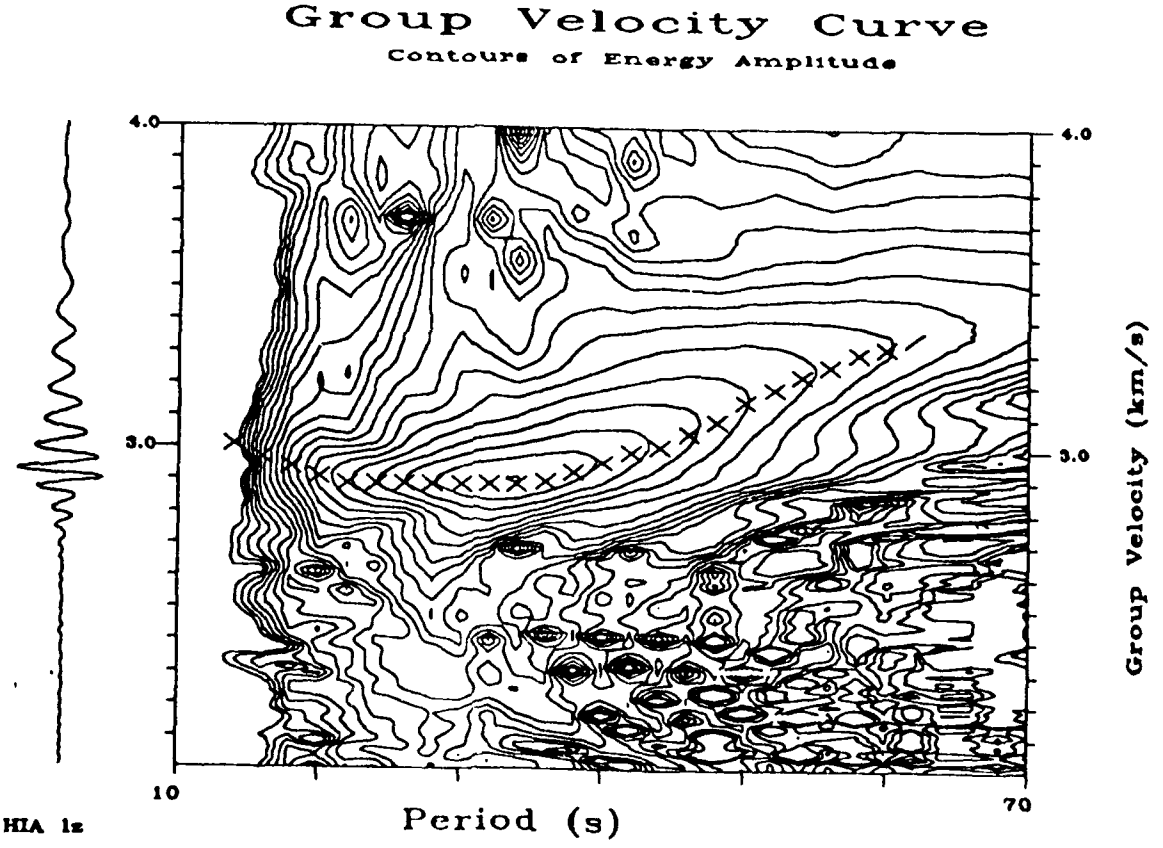

Figure 5.2.2 (b) Raleigh wave dispersion measured at HIA from an event (M_s = 4.3) in westernmost part of Xinjiang Province, China.

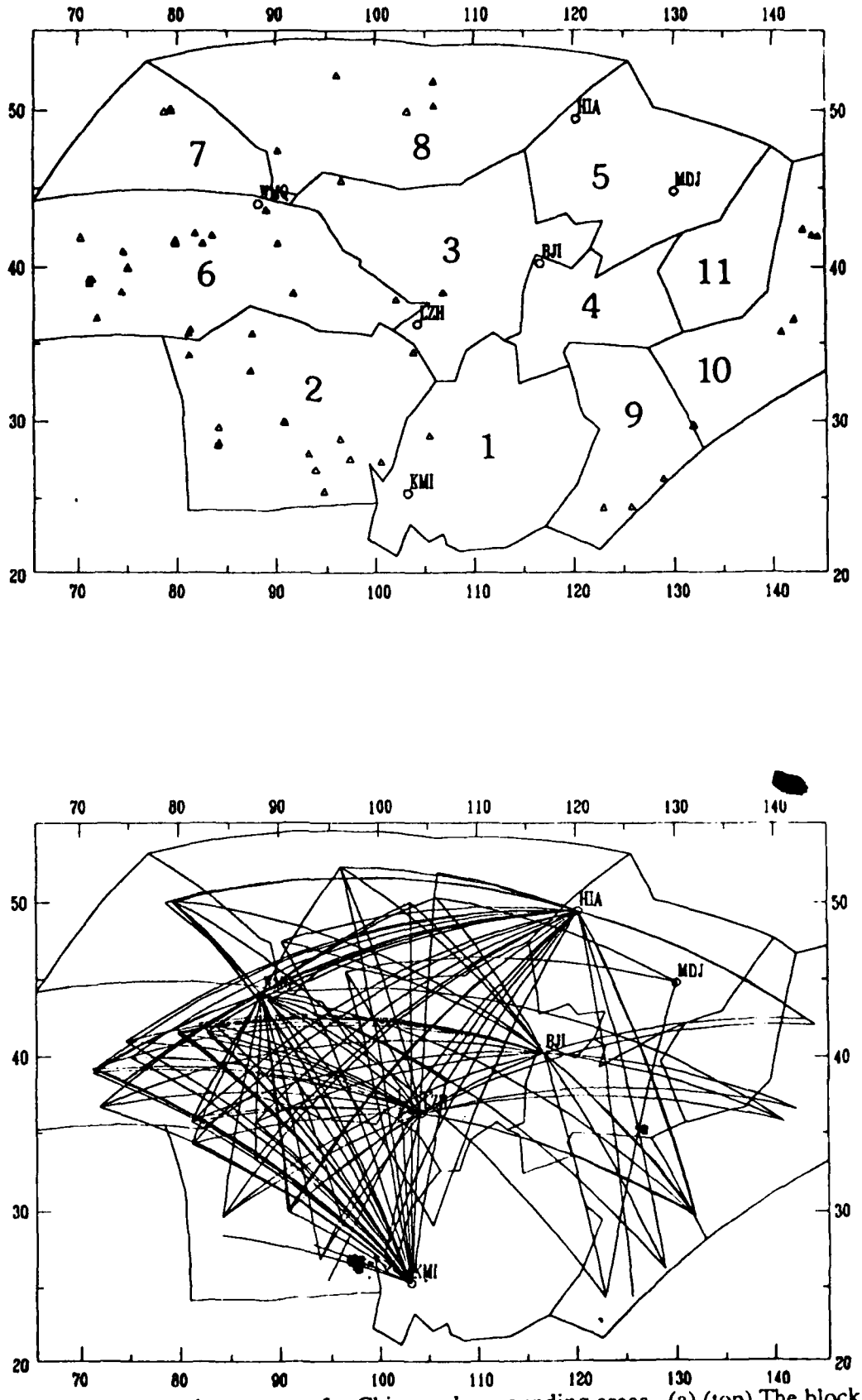

Figure 5.3.1 Simplified block structures for China and surrounding areas. (a) (top) The block numbers, the stations (circles) and location of earthquakes (triangles) are shown. (b) (bottom) The ray coverage for most of the western blocks are quite good. Blocks 9, 10, 11 are still not well traversed by the rays.

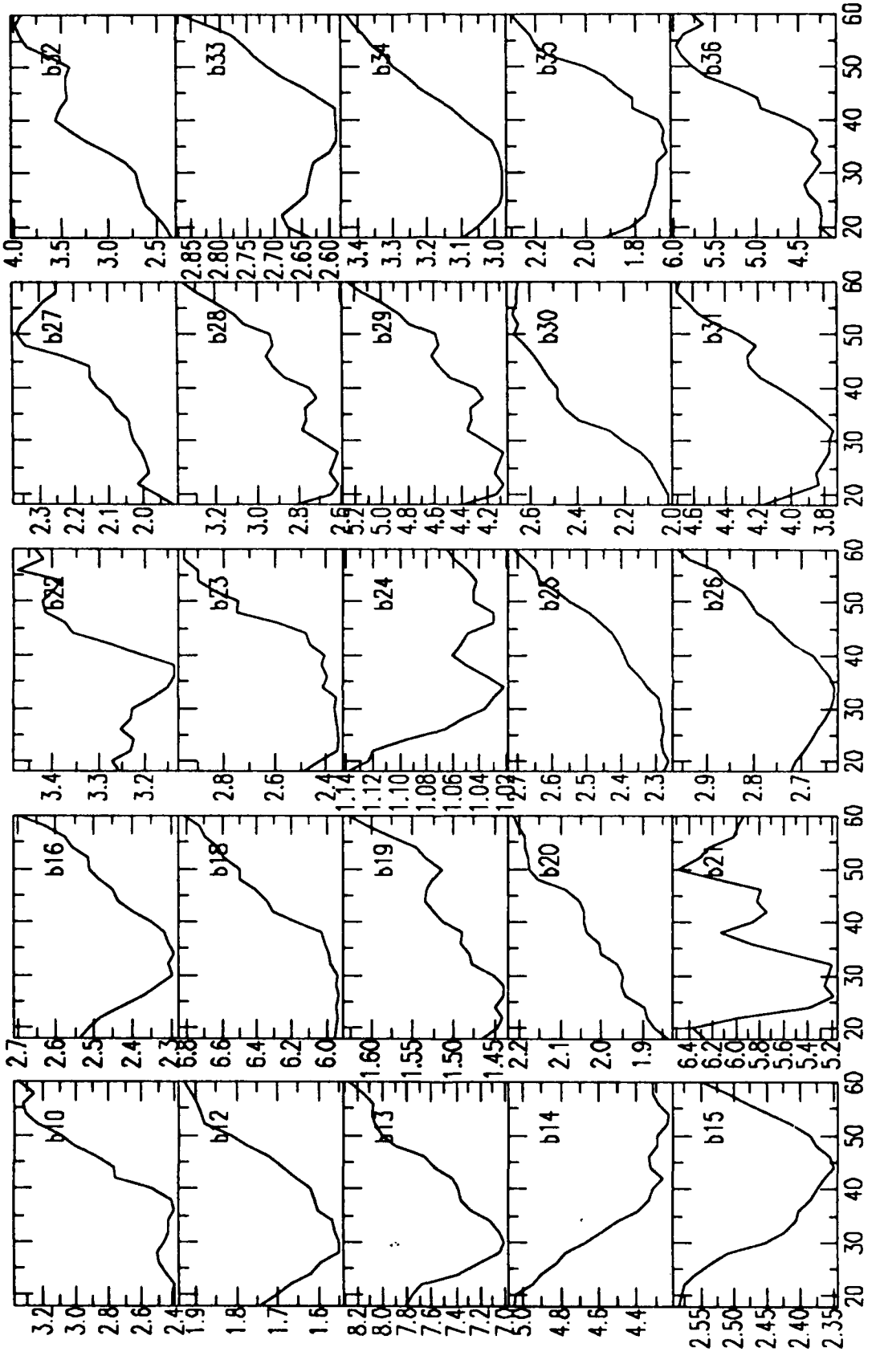

Figure 5.5.1 Regression result for the model with 37 blocks with singular cut-off at 3% of the maximum. (a) results for each block.

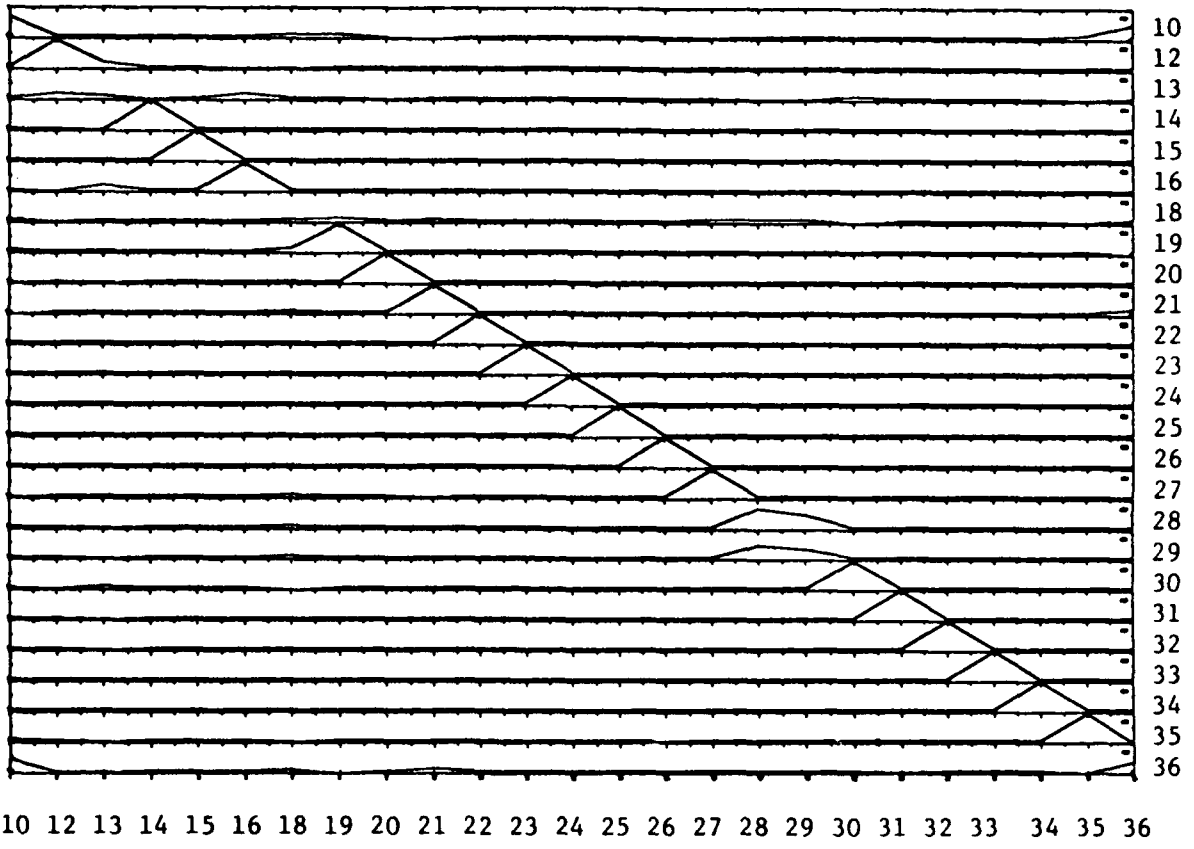

Figure 5.5.1 Regression result for the model with 37 blocks with singular cut-off at 3% of the maximum. (b) the corresponding resolution matrix. The trade-off between different blocks is severe as can be seen from from the resolution matrices.

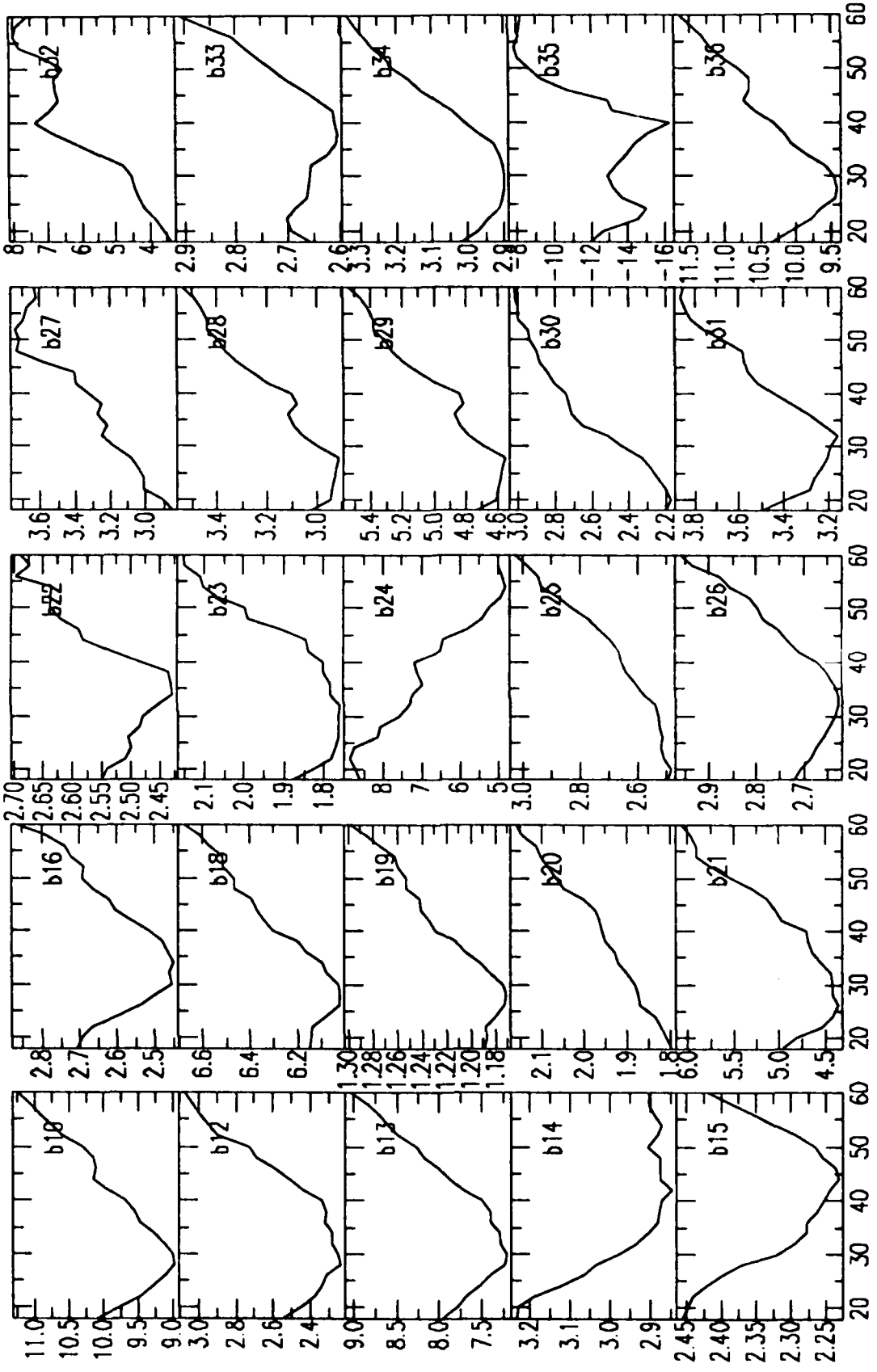

Figure 5.5.2 Regression result for the model with 37 blocks with singular cut-off at 5% of the maximum. (a) results for each block.

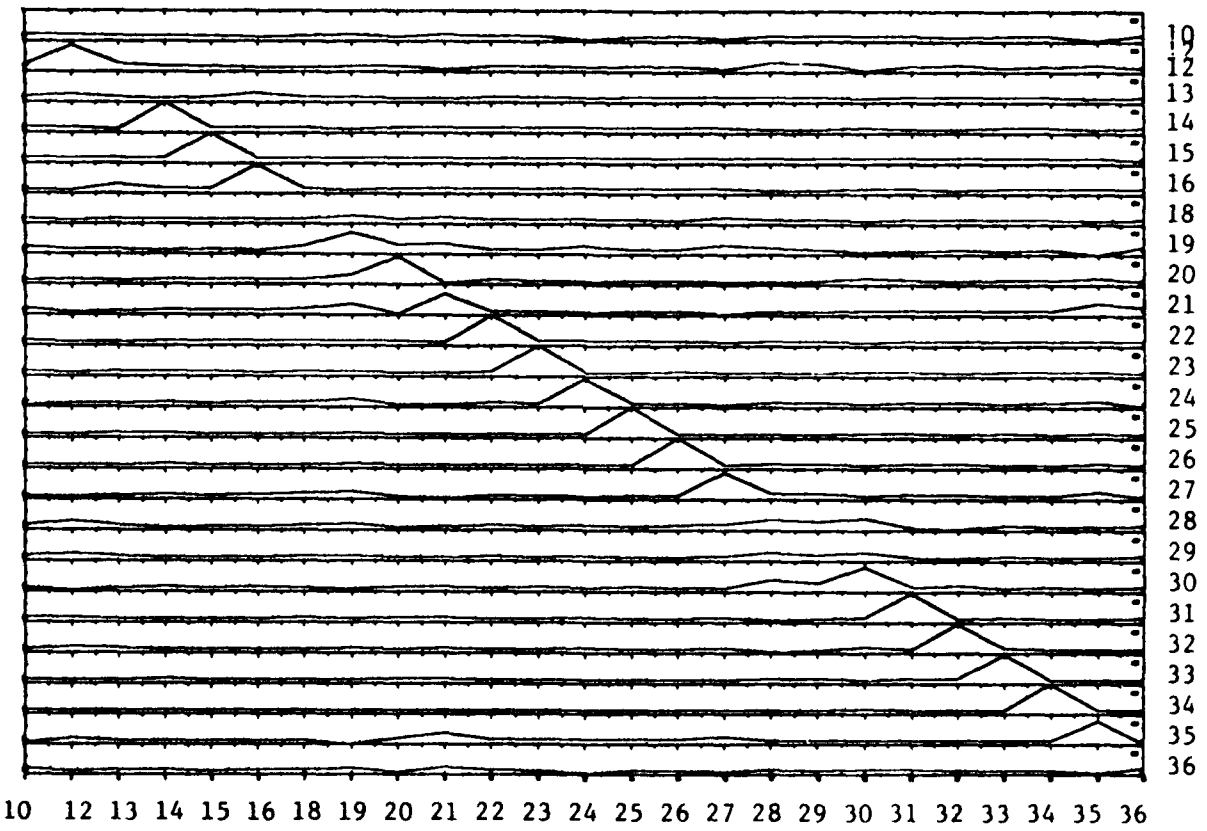

Figure 5.5.2 Regression result for the model with 37 blocks with singular cut-off at 5% of the maximum. (b) the corresponding resolution matrix. The trade-off between different blocks is severe as can be seen from from the resolution matrices.

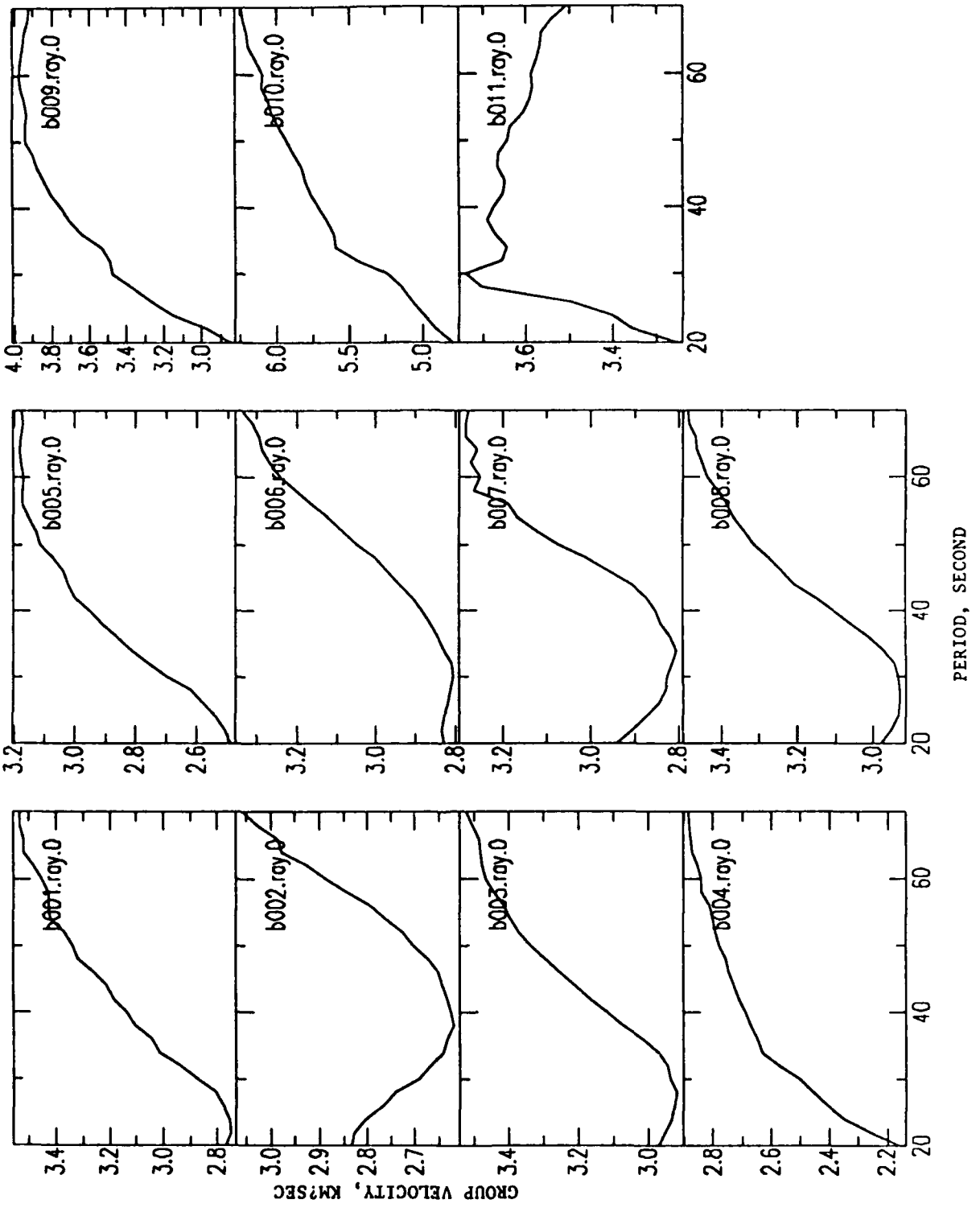

Figure 5.6.1 Rayleigh wave regression results using simplified block structures.

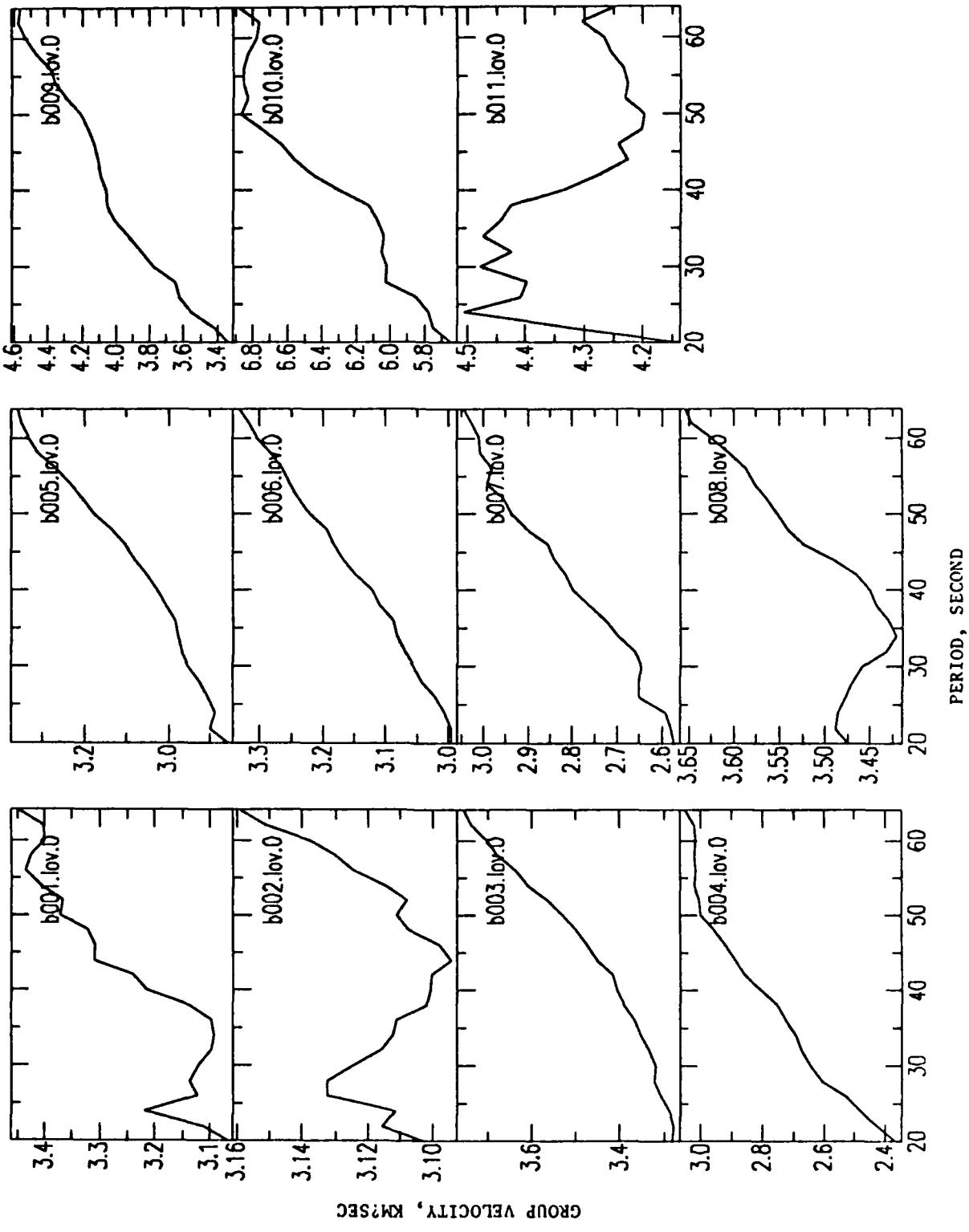

Figure 5.6.2 Love wave regression results using simplified block structures.

An inspection of these two sets of figures shows that some blocks are well resolved with stable dispersion curves. For example the result for block 15 (Tibetan plateau) is quite stable both in terms of the shape of the curves and the velocities obtained with different truncation values. Similarly, blocks 16 (the Himalayas), 20 (Alashan), 26 (Tianshan), 33 (Kazakh-Xingjiang), and 34 (Mongolia) were well resolved. These blocks are sampled by the ray paths well as can be seen in Fig. 5.2.1. The corresponding distribution of resolution matrix elements show very clearly which blocks are well sampled and which are not.

5.6 A model with fewer blocks

In order to improve resolution, we have decreased the number of blocks by combining areas of similar overall geology. For example, Tibet now includes the Kunlun Mountains and a large area dominated by Triassic sediments at the surface (Fig. 5.3.1a). For this study we have added the January through June, 1989 data. Figs. 5.3.1b shows the ray paths coverage. By simplifying the block structures we increase the ray path coverage for each block. But blocks 9, 10, and 11 are still poorly covered, and only the western part of block 1 is well covered. This occurred because data from KMI were not available during this period. Additional data from Japan, the Ryukyus and Taiwan are needed to improve the overall situation. Figs. 5.6.2 and 5.6.3 presents the Rayleigh and Love wave results. The curves are much smoother and in most cases they are well resolved. Notice that except for the blocks 9, 10 and 11, the group velocity variations are reasonable.

In order to check the validity of the results we show the KMI results for two events (9/27 and 11/3 in Table 3) in the middle of the Tibetan Plateau. The paths in this case are mostly confined with the Plateau. These two datasets (Figures 5.6.3) are nearly identical. Furthermore they agree with the regression results presented in Figs. 5.6.1 and 5.6.2. These results thus lend credence to the regression result as a whole.

5.7 Discussion

Using a year and a half of CDSN data we are able to perform initial Rayleigh and Love group velocity regionalization studies. Under the current regionaliztion scheme, the dispersion characteristics of several interesting blocks can be determined. Thus, the Tibetan plateau is seen to have a generally low velocity crust, with a minimum at 45 second. While the Tianshan velocities are higher in comparison. The Mongolian block, being an ancient (PreCambrian) shield, is shown to have rather high velocities.

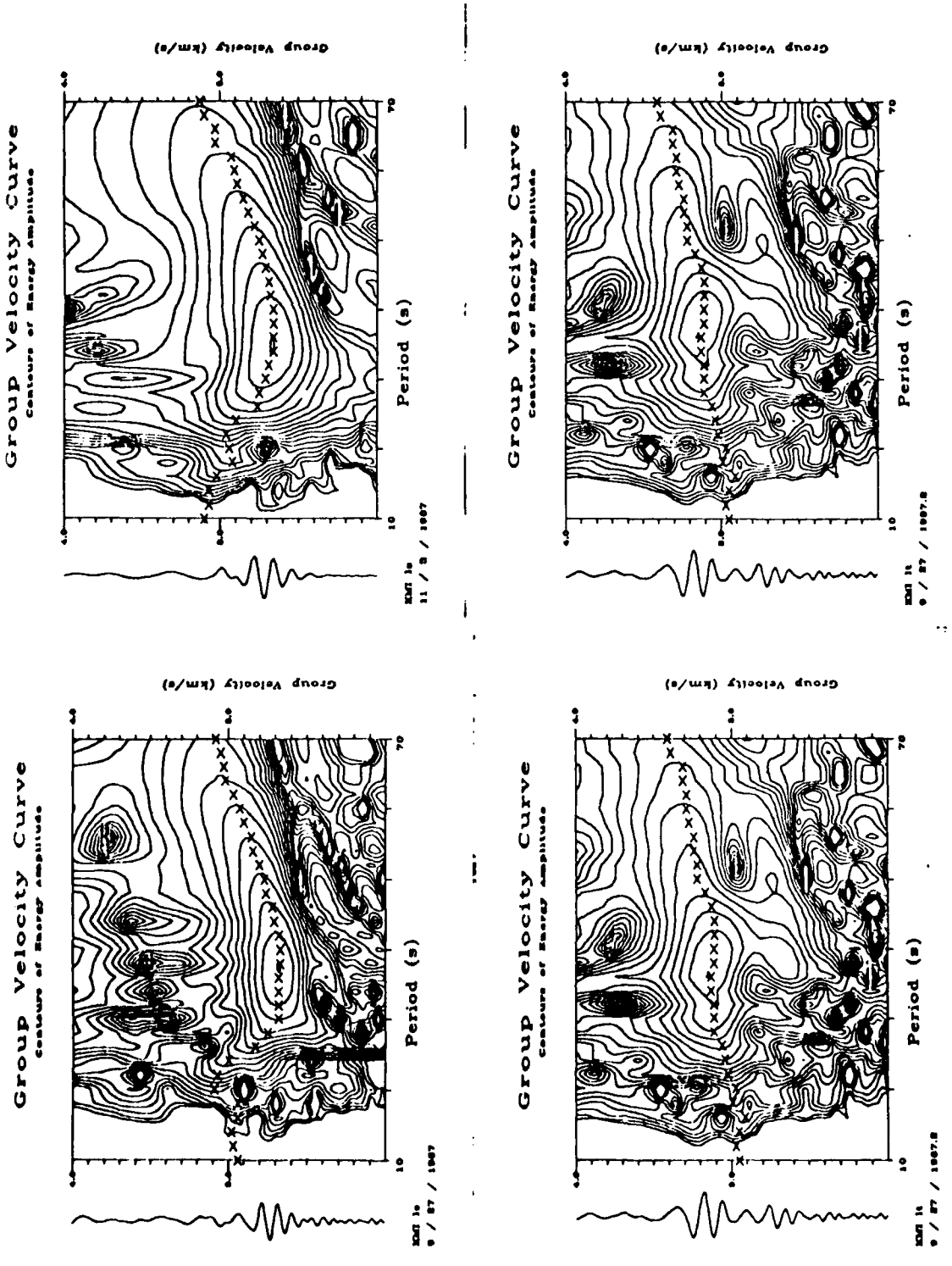

Figure 5.6.3 Rayleigh (top) and Love (bottom) group velocity curves for two events in western and central Tibet (see events on September 27 and November 3, Table 3).

Evidently, we need more data to resolve the dispersion characteristics of many blocks in the area of interest. The 1988 and 1989 events in the same source area as well as those at the continental margin to the east are being collected. We have set up our surface wave dispersion determination in such a way that we can handle a large amount of data very efficiently.

6 Acknowledgement

I would like to thank David Salzberg, who wrote the interactive group velocity determination program. This research was supported by DARPA/AFGL contract F19628-87-K-0007.

7 References

Feng, C.C. and T.L. Teng, Three dimensional crust and upper mantle structure of the Eurasian Continent, J. G. R., **88**, 2261-2272, 1983.

Burdick, L.J., C.K. Saikia, and D.V. Helmberger, Deterministic modeling of regional waveforms from the Nevada Test Sites, AFGL-TR-89-0196.

Langston, C.A., A. Lakhtakia, V.K. Varadan and V.V. Varadan, Observational and theoretical studies of regional wave propagation, 8th Annual DARPA/AFGL Seismic Research Symposium, p. 133-140, 1986.

Nishimura, C. E. and D. W. Forsyth, Rayleigh wave phase velocities in the Pacific with implications for azimuthal anisotropy and lateral heterogeneities, Geophys. J. R. Ast. Soc., **94**, 479-501, 1988.

Patton, H.J., and J.M. Mills, A study of east Kazakh explosions and propagation in Cental Asia using regional Chinese seismograms, UCID-20057, Lawrence Livermore National Laboratory, 1984.

Zhao, Y.G., Collections of Seismograms from Chinese Seismic Stations, Seismology Press, Beijing, China, 1980.

Prof. Thomas Ahrens
Seismological Lab, 252-21
Division of Geological & Planetary Sciences
California Institute of Technology
Pasadena, CA 91125

Prof. Charles B. Archambeau
CIRES
University of Colorado
Boulder, CO 80309

Prof. Muawia Barazangi
Institute for the Study of the Continent
Cornell University
Ithaca, NY 14853

Dr. Douglas R. Baumgardt
ENSCO, Inc
5400 Port Royal Road
Springfield, VA 22151-2388

Prof. Jonathan Berger
IGPP, A-025
Scripps Institution of Oceanography
University of California, San Diego
La Jolla, CA 92093

Dr. Lawrence J. Burdick
Woodward-Clyde Consultants
566 El Dorado Street
Pasadena, CA 91109-3245

Dr. Karl Coyner
New England Research, Inc.
76 Olcott Drive
White River Junction, VT 05001

Prof. Vernon F. Cormier
Department of Geology & Geophysics
U-45, Room 207
The University of Connecticut
Storrs, CT 06268

Prof. Steven Day
Department of Geological Sciences
San Diego State University
San Diego, CA 92182

Dr. Zoltan A. Der
ENSCO, Inc.
5400 Port Royal Road
Springfield, VA 22151-2388

Prof. John Ferguson
Center for Lithospheric Studies
The University of Texas at Dallas
P.O. Box 830688
Richardson, TX 75083-0688

Prof. Stanley Flatte
Applied Sciences Building
University of California
Santa Cruz, CA 95064

Dr. Alexander Florence
SRI International
333 Ravenswood Avenue
Menlo Park, CA 94025-3493

Prof. Henry L. Gray
Vice Provost and Dean
Department of Statistical Sciences
Southern Methodist University
Dallas, TX 75275

Dr. Indra Gupta
Teledyne Geotech
314 Montgomery Street
Alexandria, VA 22314

Prof. David G. Harkrider
Seismological Laboratory
Division of Geological & Planetary Sciences
California Institute of Technology
Pasadena, CA 91125

Prof. Donald V. Helmberger
Seismological Laboratory
Division of Geological & Planetary Sciences
California Institute of Technology
Pasadena, CA 91125

Prof. Eugene Herrin
Institute for the Study of Earth and Man
GeophysicalLaboratory
Southern Methodist University
Dallas, TX 75275

Prof . Robert B. Herrmann
Department of Earth & Atmospheric Sciences
St. Louis University
St. Louis, MO 63156

Prof. Bryan Isacks
Cornell University
Department of Geological Sciences
SNEE Hall
Ithaca, NY 14850

Dr. Rong-Song Jih
Teledyne Geotech
314 Montgomery Street
Alexandria, VA 22314

Prof. Lane R. Johnson
Seismographic Station
University of California
Berkeley, CA 94720

Prof. Alan Kafka
Department of Geology & Geophysics
Boston College
Chestnut Hill, MA 02167

Prof. Fred K. Lamb
University of Illinois at Urbana-Champaign
Department of Physics
1110 West Green Street
Urbana, IL 61801

Prof. Charles A. Langston
Geosciences Department
403 Deike Building
The Pennsylvania State University
University Park, PA 16802

Professor Thorne Lay
Institute of Tectonics
Earth Science Board
University of California, Santa Cruz
Santa Cruz, CA 95064

Prof. Arthur Lerner-Lam
Lamont-Doherty Geological Observatory
of Columbia University
Palisades, NY 10964

Dr. Christopher Lynnes
Teledyne Geotech
314 Montgomery Street
Alexandria, VA 22314

Prof. Peter Malin
University of California at Santa Barbara
Institute for Crustal Studies
Santa Barbara, CA 93106

Dr. Randolph Martin, III
New England Research, Inc.
76 Olcott Drive
White River Junction, VT 05001

Dr. Gary McCartor
Mission Research Corporation
735 State Street
P.O. Drawer 719
Santa Barbara, CA 93102 (2 copies)

Prof. Thomas V. McEvilly
Seismographic Station
University of California
Berkeley, CA 94720

Dr. Keith L. McLaughlin
S-CUBED
A Division of Maxwell Laboratory
P.O. Box 1620
La Jolla, CA 92038-1620

Prof. William Menke
Lamont-Doherty Geological Observatory
of Columbia University
Palisades, NY 10964

Stephen Miller
SRI International
333 Ravenswood Avenue
Box AF 116
Menlo Park, CA 94025-3493

Prof. Bernard Minster
IGPP, A-025
Scripps Institute of Oceanography
University of California, San Diego
La Jolla, CA 92093

Prof. Brian J. Mitchell
Department of Earth & Atmospheric Sciences
St. Louis University
St. Louis, MO 63156

Mr. Jack Murphy
S-CUBED, A Division of Maxwell Laboratory
11800 Sunrise Valley Drive
Suite 1212
Reston, VA 22091 (2 copies)

Dr. Bao Nguyen
GL/LWH
Hanscom AFB, MA 01731-5000

Prof. John A. Orcutt
IGPP, A-025
Scripps Institute of Oceanography
University of California, San Diego
La Jolla, CA 92093

Prof. Keith Priestley
University of Nevada
Mackay School of Mines
Reno, NV 89557

Prof. Paul G. Richards
Lamont-Doherty Geological Observatory
of Columbia University
Palisades, NY 10964

Dr. Wilmer Rivers
Teledyne Geotech
314 Montgomery Street
Alexandria, VA 22314

Dr. Alan S. Ryall, Jr.
Center for Seismic Studies
1300 North 17th Street
Suite 1450
Arlington, VA 22209-2308

Prof. Charles G. Sammis
Center for Earth Sciences
University of Southern California
University Park
Los Angeles, CA 90089-0741

Prof. Christopher H. Scholz
Lamont-Doherty Geological Observatory
of Columbia University
Palisades, NY 10964

Prof. David G. Simpson
Lamont-Doherty Geological Observatory
of Columbia University
Palisades, NY 10964

Dr. Jeffrey Stevens
S-CUBED
A Division of Maxwell Laboratory
P.O. Box 1620
La Jolla, CA 92038-1620

Prof. Brian Stump
Institute for the Study of Earth & Man
Geophysical Laboratory
Southern Methodist University
Dallas, TX 75275

Prof. Jeremiah Sullivan
University of Illinois at Urbana-Champaign
Department of Physics
1110 West Green Street
Urbana, IL 61801

Prof. Clifford Thurber
University of Wisconsin-Madison
Department of Geology & Geophysics
1215 West Dayton Street
Madison, WS 53706

Prof. M. Nafi Toksoz
Earth Resources Lab
Massachusetts Institute of Technology
42 Carleton Street
Cambridge, MA 02142

Prof. John E. Vidale
University of California at Santa Cruz
Seismological Laboratory
Santa Cruz, CA 95064

Prof. Terry C. Wallace
Department of Geosciences
Building #77
University of Arizona
Tucson, AZ 85721

Dr. Raymond Willeman
GL/LWH
Hanscom AFB, MA 01731-5000

Dr. Lorraine Wolf
GL/LWH
Hanscom AFB, MA 01731-5000

Prof. Francis T. Wu
Department of Geological Sciences
State University of New York
at Binghamton
Vestal, NY 13901

OTHERS (United States)

Dr. Monem Abdel-Gawad
Rockwell International Science Center
1049 Camino Dos Rios
Thousand Oaks, CA 91360

Prof. Keiiti Aki
Center for Earth Sciences
University of Southern California
University Park
Los Angeles, CA 90089-0741

Prof. Shelton S. Alexander
Geosciences Department
403 Deike Building
The Pennsylvania State University
University Park, PA 16802

Dr. Ralph Archuleta
Department of Geological Sciences
University of California at Santa Barbara
Santa Barbara, CA 93102

Dr. Thomas C. Bache, Jr.
Science Applications Int'l Corp.
10210 Campus Point Drive
San Diego, CA 92121 (2 copies)

J. Barker
Department of Geological Sciences
State University of New York
at Binghamton
Vestal, NY 13901

Dr. T.J. Bennett
S-CUBED
A Division of Maxwell Laboratory
11800 Sunrise Valley Drive, Suite 1212
Reston, VA 22091

Mr. William J. Best
907 Westwood Drive
Vienna, VA 22180

Dr. N. Biswas
Geophysical Institute
University of Alaska
Fairbanks, AK 99701

Dr. G.A. Bollinger
Department of Geological Sciences
Virginia Polytechnical Institute
21044 Derring Hall
Blacksburg, VA 24061

Dr. Stephen Bratt
Science Applications Int'l Corp.
10210 Campus Point Drive
San Diego, CA 92121

Michael Browne
Teledyne Geotech
3401 Shiloh Road
Garland, TX 75041

Mr. Roy Burger
1221 Serry Road
Schenectady, NY 12309

Dr. Robert Burridge
Schlumberger-Doll Research Center
Old Quarry Road
Ridgefield, CT 06877

Dr. Jerry Carter
Rondout Associates
P.O. Box 224
Stone Ridge, NY 12484

Dr. W. Winston Chan
Teledyne Geotech
314 Montgomery Street
Alexandria, VA 22314-1581

Dr. Theodore Cherry
Science Horizons, Inc.
710 Encinitas Blvd., Suite 200
Encinitas, CA 92024 (2 copies)

Prof. Jon F. Claerbout
Department of Geophysics
Stanford University
Stanford, CA 94305

Prof. Robert W. Clayton
Seismological Laboratory
Division of Geological & Planetary Sciences
California Institute of Technology
Pasadena, CA 91125

Prof. F. A. Dahlen
Geological and Geophysical Sciences
Princeton University
Princeton, NJ 08544-0636

Prof. Anton W. Dainty
Earth Resources Lab
Massachusetts Institute of Technology
42 Carleton Street
Cambridge, MA 02142

Prof. Adam Dziewonski
Hoffman Laboratory
Harvard University
20 Oxford St
Cambridge, MA 02138

Prof. John Ebel
Department of Geology & Geophysics
Boston College
Chestnut Hill, MA 02167

Eric Fielding
SNEE Hall
INSTOC
Cornell University
Ithaca, NY 14853

Prof. Donald Forsyth
Department of Geological Sciences
Brown University
Providence, RI 02912

Prof. Art Frankel
Mail Stop 922
Geological Survey
790 National Center
Reston, VA 22092

Dr. Anthony Gangi
Texas A&M University
Department of Geophysics
College Station, TX 77843

Dr. Freeman Gilbert
Inst. of Geophysics & Planetary Physics
University of California, San Diego
P.O. Box 109
La Jolla, CA 92037

Mr. Edward Giller
Pacific Sierra Research Corp.
1401 Wilson Boulevard
Arlington, VA 22209

Dr. Jeffrey W. Given
Sierra Geophysics
11255 Kirkland Way
Kirkland, WA 98033

Prof. Stephen Grand
University of Texas at Austin
Department of Geological Sciences
Austin, TX 78713-7909

Prof. Roy Greenfield
Geosciences Department
403 Deike Building
The Pennsylvania State University
University Park, PA 16802

Dan N. Hagedorn
Battelle
Pacific Northwest Laboratories
Battelle Boulevard
Richland, WA 99352

Kevin Hutchenson
Department of Earth Sciences
St. Louis University
3507 Laclede
St. Louis, MO 63103

Prof. Thomas H. Jordan
Department of Earth, Atmospheric
and Planetary Sciences
Massachusetts Institute of Technology
Cambridge, MA 02139

Robert C. Kemerait
ENSCO, Inc.
445 Pineda Court
Melbourne, FL 32940

William Kikendall
Teledyne Geotech
3401 Shiloh Road
Garland, TX 75041

Prof. Leon Knopoff
University of California
Institute of Geophysics & Planetary Physics
Los Angeles, CA 90024

Prof. L. Timothy Long
School of Geophysical Sciences
Georgia Institute of Technology
Atlanta, GA 30332

Prof. Art McGarr
Mail Stop 977
Geological Survey
345 Middlefield Rd.
Menlo Park, CA 94025

Dr. George Mellman
Sierra Geophysics
11255 Kirkland Way
Kirkland, WA 98033

Prof. John Nabelek
College of Oceanography
Oregon State University
Corvallis, OR 97331

Prof. Geza Nagy
University of California, San Diego
Department of Ames, M.S. B-010
La Jolla, CA 92093

Prof. Amos Nur
Department of Geophysics
Stanford University
Stanford, CA 94305

Prof. Jack Oliver
Department of Geology
Cornell University
Ithaca, NY 14850

Prof. Robert Phinney
Geological & Geophysical Sciences
Princeton University
Princeton, NJ 08544-0636

Dr. Paul Pomeroy
Rondout Associates
P.O. Box 224
Stone Ridge, NY 12484

Dr. Jay Pulli
RADIX System, Inc.
2 Taft Court, Suite 203
Rockville, MD 20850

Dr. Norton Rimer
S-CUBED
A Division of Maxwell Laboratory
P.O. Box 1620
La Jolla, CA 92038-1620

Prof. Larry J. Ruff
Department of Geological Sciences
1006 C.C. Little Building
University of Michigan
Ann Arbor, MI 48109-1063

Dr. Richard Sailor
TASC Inc.
55 Walkers Brook Drive
Reading, MA 01867

Thomas J. Sereno, Jr.
Science Application Int'l Corp.
10210 Campus Point Drive
San Diego, CA 92121

John Sherwin
Teledyne Geotech
3401 Shiloh Road
Garland, TX 75041

Prof. Robert Smith
Department of Geophysics
University of Utah
1400 East 2nd South
Salt Lake City, UT 84112

Prof. S. W. Smith
Geophysics Program
University of Washington
Seattle, WA 98195

Dr. Stewart Smith
IRIS Inc.
1616 North Fort Myer Drive
Suite 1440
Arlington, VA 22209

Dr. George Sutton
Rondout Associates
P.O. Box 224
Stone Ridge, NY 12484

Prof. L. Sykes
Lamont-Doherty Geological Observatory
of Columbia University
Palisades, NY 10964

Prof. Pradeep Talwani
Department of Geological Sciences
University of South Carolina
Columbia, SC 29208

Prof. Ta-liang Teng
Center for Earth Sciences
University of Southern California
University Park
Los Angeles, CA 90089-0741

Dr. R.B. Tittmann
Rockwell International Science Center
1049 Camino Dos Rios
P.O. Box 1085
Thousand Oaks, CA 91360

Dr. Gregory van der Vink
IRIS, Inc.
1616 North Fort Myer Drive
Suite 1440
Arlington, VA 22209

William R. Walter
Seismological Laboratory
University of Nevada
Reno, NV 89557

Dr. Gregory Wojcik
Weidlinger Associates
4410 El Camino Real
Suite 110
Los Altos, CA 94022

Prof. John H. Woodhouse
Hoffman Laboratory
Harvard University
20 Oxford Street
Cambridge, MA 02138

Dr. Gregory B. Young
ENSCO, Inc.
5400 Port Royal Road
Springfield, VA 22151-2388

GOVERNMENT

Dr. Ralph Alewine III
DARPA/NMRO
1400 Wilson Boulevard
Arlington, VA 01731-5000

Mr. James C. Battis
GL/LWH
Hanscom AFB, MA 22209-2308

Dr. Robert Blandford
DARPA/NMRO
1400 Wilson Boulevard
Arlington, VA 87185

Eric Chael
Division 9241
Sandia Laboratory
Albuquerque, NM 01731-5000

Dr. John J. Cipar
GL/LWH
Hanscom AFB, MA 01731-5000

Mr. Jeff Duncan
Office of Congressman Markey
2133 Rayburn House Bldg.
Washington, D.C. 20515

Dr. Jack Evernden
USGS - Earthquake Studies
345 Middlefield Road
Menlo Park, CA 94025

Art Frankel
USGS
922 National Center
Reston, VA 22092

Dr. T. Hanks
USGS
Nat'l Earthquake Research Center
345 Middlefield Road
Menlo Park, CA 94025

Dr. James Hannon
Lawrence Livermore Nat'l Laboratory
P.O. Box 808
Livermore, CA 94550

Paul Johnson
ESS-4, Mail Stop J979
Los Alamos National Laboratory
Los Alamos, NM 87545

Janet Johnston
GL/LWH
Hanscom AFB, MA 01731-5000

Dr. Katharine Kadinsky-Cade
GL/LWH
Hanscom AFB, MA 01731-5000

Ms. Ann Kerr
IGPP, A-025
Scripps Institute of Oceanography
University of California, San Diego
La Jolla, CA 92093

Dr. Max Koontz
US Dept of Energy/DP 5
Forrestal Building
1000 Independence Avenue
Washington, DC 20585

Dr. W.H.K. Lee
Office of Earthquakes, Volcanoes,
& Engineering
345 Middlefield Road
Menlo Park, CA 94025

Dr. William Leith
U.S. Geological Survey
Mail Stop 928
Reston, VA 22092

Dr. Richard Lewis
Director, Earthquake Engineering & Geophysics
U.S. Army Corps of Engineers
Box 631
Vicksburg, MS 39180

James F. Lewkowicz
GL/LWH
Hanscom AFB, MA 01731-5000

Mr. Alfred Lieberman
ACDA/VI-OA'State Department Bldg
Room 5726
320 - 21st Street, NW
Washington, DC 20451

Stephen Mangino
GL/LWH
Hanscom AFB, MA 01731-5000

Dr. Robert Masse
Box 25046, Mail Stop 967
Denver Federal Center
Denver, CO 80225

Art McGarr
U.S. Geological Survey, MS-977
345 Middlefield Road
Menlo Park, CA 94025

Richard Morrow
ACDA/VI, Room 5741
320 21st Street N.W
Washington, DC 20451

Dr. Keith K. Nakanishi
Lawrence Livermore National Laboratory
P.O. Box 808, L-205
Livermore, CA 94550

Dr. Carl Newton
Los Alamos National Laboratory
P.O. Box 1663
Mail Stop C335, Group ESS-3
Los Alamos, NM 87545

Dr. Kenneth H. Olsen
Los Alamos Scientific Laboratory
P.O. Box 1663
Mail Stop C335, Group ESS-3
Los Alamos, NM 87545

Howard J. Patton
Lawrence Livermore National Laboratory
P.O. Box 808, L-205
Livermore, CA 94550

Mr. Chris Paine
Office of Senator Kennedy, SR 315

United States Senate
Washington, DC 20510

Colonel Jerry J. Perrizo
AFOSR/NP, Building 410
Bolling AFB
Washington, DC 20332-6448

Dr. Frank F. Pilotte
HQ AFTAC/TT
Patrick AFB, FL 32925-6001

Katie Poley
CIA-OSWR/NED
Washington, DC 20505

Mr. Jack Rachlin
U.S. Geological Survey
Geology, Rm 3 C136
Mail Stop 928 National Center
Reston, VA 22092

Dr. Robert Reinke
WL/NTESG
Kirtland AFB, NM 87117-6008

Dr. Byron Ristvet
HQ DNA, Nevada Operations Office
Attn: NVCG
P.O. Box 98539
Las Vegas, NV 89193

Dr. George Rothe
HQ AFTAC/TGR
Patrick AFB, FL 32925-6001

Dr. Michael Shore
Defense Nuclear Agency/SPSS
6801 Telegraph Road
Alexandria, VA 22310

Donald L. Springer
Lawrence Livermore National Laboratory
P.O. Box 808, L-205
Livermore , CA 94550

Dr. Lawrence Turnbull
OSWR/NED
Central Intelligence Agency, Room 5G48
Washington, DC 20505

Dr. Thomas Weaver
Los Alamos National Laboratory
P.O. Box 1663, Mail Stop C335
Los Alamos, NM 87545

J.J. Zucca
Lawrence Livermore National Laboratory
Box 808
Livermore, CA 94550

GL/SULL
Research Library
Hanscom AFB , MA 01731-5000 (2 copies)

Secretary of the Air Force (SAFRD)

Washington, DC 20330

Office of the Secretary Defense
DDR & E
Washington, DC 20330

HQ DNA
Attn: Technical Library
Washington, DC 20305

DARPA/RMO/RETRIEVAL
1400 Wilson Boulevard
Arlington, VA 22209

DARPA/RMO/Security Office
1400 Wilson Boulevard
Arlington, VA 22209

Geophysics Laboratory
Attn: XO
Hanscom AFB, MA 01731-5000

Geophysics Laboratory
Attn: LW
Hanscom AFB, MA 01731-5000

DARPA/PM
1400 Wilson Boulevard
Arlington, VA 22209

Defense Technical Information Center
Cameron Station
Alexandria, VA 22314 (5 copies)

Defense Intelligence Agency
Directorate for Scientific &
Technical Intelligence
Washington, DC 20301

AFTAC/CA
(STINFO)
Patrick AFB, FL 32925-6001

TACTEC
Battelle Memorial Institute
505 King Avenue
Columbus, OH 43201 (Final Report Only)

Mr. Charles L. Taylor
GL/LWH

Hanscom AFB, MA 01731-5000

Dr. Ramon Cabre, S.J.
Observatorio San Calixto
Casilla 5939
La Paz, Bolivia

Prof. Hans-Peter Harjes
Institute for Geophysik
Ruhr University/Bochum
P.O. Box 102148
4630 Bochum 1, FRG

Prof. Eystein Husebye
NTNF/NORSAR
P.O. Box 51
N-2007 Kjeller, NORWAY

Prof. Brian L.N. Kennett
Research School of Earth Sciences
Institute of Advanced Studies
G.P.O. Box 4
Canberra 2601, AUSTRALIA

Dr. Bernard Massinon
Societe Radiomana
27 rue Claude Bernard
75005 Paris, FRANCE (2 Copies)

Dr. Pierre Mecheler
Societe Radiomana
27 rue Claude Bernard
75005 Paris, FRANCE

Dr. Svein Mykkeltveit
NTNF/NORSAR
P.O. Box 51
N-2007 Kjeller, NORWAY

FOREIGN (Others)

Dr. Peter Basham
Earth Physics Branch
Geological Survey of Canada
1 Observatory Crescent
Ottawa, Ontario, CANADA K1A 0Y3

Dr. Eduard Berg
Institute of Geophysics
University of Hawaii
Honolulu, HI 96822

Dr. Michel Bouchon
I.R.I.G.M.-B.P. 68
38402 St. Martin D'Heres
Cedex, FRANCE

Dr. Hilmar Bungum
NTNF/NORSAR
P.O. Box 51
N-2007 Kjeller, NORWAY

Dr. Michel Campillo
Observatoire de Grenoble
I.R.I.G.M.-B.P. 53
38041 Grenoble, FRANCE

Dr. Kin Yip Chun
Geophysics Division
Physics Department
University of Toronto
Ontario, CANADA M5S 1A7

Dr. Alan Douglas
Ministry of Defense
Blacknest, Brimpton
Reading RG7-4RS, UNITED KINGDOM

Dr. Roger Hansen
NTNF/NORSAR
P.O. Box 51
N-2007 Kjeller, NORWAY

Dr. Manfred Henger
Federal Institute for Geosciences & Nat'l Res.
Postfach 510153
D-3000 Hanover 51, FRG

Ms. Eva Johannisson
Senior Research Officer
National Defense Research Inst.
P.O. Box 27322
S-102 54 Stockholm, SWEDEN

Dr. Fekadu Kebede
Seismological Section
Box 12019
S-750 Uppsala, SWEDEN

Dr. Tormod Kvaerna
NTNF/NORSAR
P.O. Box 51
N-2007 Kjeller, NORWAY

Dr. Peter Marshal
Procurement Executive
Ministry of Defense
Blacknest, Brimpton
Reading FG7-4RS, UNITED KINGDOM

Prof. Ari Ben-Menahem
Department of Applied Mathematics
Weizman Institute of Science
Rehovot, ISRAEL 951729

Dr. Robert North
Geophysics Division
Geological Survey of Canada
1 Observatory Crescent
Ottawa, Ontario, CANADA K1A 0Y3

Dr. Frode Ringdal
NTNF/NORSAR
P.O. Box 51
N-2007 Kjeller, NORWAY

Dr. Jorg Schlittenhardt
Federal Institute for Geosciences & Nat'l Res.
Postfach 510153
D-3000 Hannover 51, FEDERAL REPUBLIC OF GERMANY

Prof. Daniel Walker
University of Hawaii
Institute of Geophysics
Honolulu, HI 96822